

Electronic Thesis and Dissertation Repository

5-10-2017 12:00 AM

Estimation of cavity pressures in air-permeable, multi-layer systems using a lumped-leakage approach

Rahul Prabhakaran Nair Sreedevi
The University of Western Ontario

Supervisor
Gregory A Kopp
The University of Western Ontario

Graduate Program in Civil and Environmental Engineering
A thesis submitted in partial fulfillment of the requirements for the degree in Master of Engineering Science
© Rahul Prabhakaran Nair Sreedevi 2017

Follow this and additional works at: <https://ir.lib.uwo.ca/etd>



Part of the [Civil Engineering Commons](#)

Recommended Citation

Prabhakaran Nair Sreedevi, Rahul, "Estimation of cavity pressures in air-permeable, multi-layer systems using a lumped-leakage approach" (2017). *Electronic Thesis and Dissertation Repository*. 4549.
<https://ir.lib.uwo.ca/etd/4549>

This Dissertation/Thesis is brought to you for free and open access by Scholarship@Western. It has been accepted for inclusion in Electronic Thesis and Dissertation Repository by an authorized administrator of Scholarship@Western. For more information, please contact wlsadmin@uwo.ca.

Abstract

For conventional buildings, the proper estimation of wind-induced pressures on the external façade, the roof surface, or the net pressures across elements like a canopy or parapet, which are exposed to wind on both sides, can be easily done using conventional wind tunnel tests. But in the case of air-permeable multi-layer systems, which have gaps or porosity in the external layer along with a cavity between the external and inner layers, the estimation of wind loading across the external layer or in the inner cavity by wind tunnel tests can be quite difficult due to practical difficulties in exactly simulating the dimensions of the gaps in the physical model with small model scales or other practical issues related to the tubing of the pressure sensors.

Pressure equalization plays a major role on the wind loading on individual members of multi-layer systems and in this study, an analytical model to estimate the time-varying cavity pressure distributions in a double-layer system with an air-permeable outer layer was developed, given the external pressure on the outer surface. The pressure drop associated with the flow through the gaps in the external layer was modeled using orifice flow equation and mass conservation equation (Oh, J.H. & Kopp, G.A., 2014). The model accounts the geometric parameters like the cavity depth (H) which is the distance between the outer layer and the inner non-porous layer along with loss coefficient for the orifice flow through the gaps in the external layer. Moreover, the pressure drop due to flow through the gaps (G) in the external layer are accounted based on a lumped-leakage approach. The results from the analytical model are compared with wind-induced loads obtained from the wind tunnel test of roof-mounted photovoltaic solar array system with high G/H ratio obtained from Stenabaugh (2015).

Keywords

Wind loading, Pressure equalization, air-permeable cladding, building aerodynamics.

Co-Authorship Statement

This work was done based on the valuable inputs and suggestion from Dr. Gregory Kopp, who was very helpful and encouraging. Under his guidance, I developed the analytical model using basic equations from Oh, J., & Kopp, G. (2014). Sarah Stenabaugh was kind enough to provide me the wind tunnel results from her doctoral experiments (Stenabaugh, S., (2015)) for the validation of results obtained from my analytical model. All of her data has been cited and her generosity is appreciated.

Acknowledgments

Actually I am grateful and beholden to many people and here I am mentioning only a few from that big list.

First and foremost, I would like to thank my supervisor Dr. Gregory Kopp for giving me this opportunity to pursue this research and for all the encouragement, support, generosity and guidance. I immensely appreciate all his contributions in terms of time, ideas and also funding which made my whole experience in Western University very productive. I am thankful for the enthusiasm and motivation, he gave me throughout the last 2 years and also for the excellent ideas he has provided which helped me academically as well as in my future professional life.

I would like to express my special thanks and gratitude to Sarah Stenabaugh for providing me the data needed for the validation of my analytical model.

The students in our Wind Engineering group, especially Emilio, Sarah, Arif, and Anant have contributed immensely to my personal and professional time and I am indebted to all of them for being such good friends. This thesis work would have not been possible without the kind assistance provided by Chieh-Hsun on Matlab programming. Thank you for teaching me the basics of Matlab as well as for all the solicited inputs and advices. Special thanks to Sibin for helping me in Matlab.

To my loving family without whom this journey would not have been possible. Thank you for all your prayers and my apologies for always keeping you worried about my well-being. The generous support from all the professors in Wind Engineering is gratefully acknowledged. Last but not the least, thank you to all my RWDI friends for making me what I am today.

Table of Contents

Abstract	ii
Co-Authorship Statement.....	iii
Acknowledgments.....	iv
Table of Contents	v
List of Tables	viii
List of Figures	ix
List of Appendices	xiii
Nomenclature	xiv
Chapter 1	1
1 Introduction	1
1.1 Background.....	2
1.2 Analytical models in literature.....	5
1.3 Previous studies on loose-laid pavers	7
1.4 Previous studies on roof-mounted solar panels	8
1.5 Previous studies on porous and rainscreen systems.....	11
1.6 Objective of the thesis.....	14
Chapter 2.....	15
2 Analytical modeling for the estimation of cavity pressure	15
2.1 Introduction.....	15
2.2 Mathematical Formulation.....	15
2.2.1 Equations for flow through an orifice.....	15
2.2.2 Concept of neutral pressure line	17
2.2.3 Equations for flow through multiple openings	18

2.2.4	Assumptions considered in the proposed analytical model	21
2.2.5	Analytical model for estimating the cavity pressure using a lumped-leakage approach.....	23
2.3	Details of the numerical simulation	27
Chapter 3	29
3	Results and Discussion.....	29
3.1	Introduction.....	29
3.2	Experimental set-up	29
3.3	Assumptions considered in the analytical model.....	33
3.3.1	Validation of the assumptions considered in the analytical model.....	33
3.4	Method	39
3.4.1	Consideration of simplified areas as input for the model	41
3.5	Results.....	43
3.5.1	Comparison of time-series and spectra of area-averaged pressure coefficients.....	43
3.5.2	Comparison of predicted cavity pressure time-series with individual cavity pressure tap time series	49
3.5.3	Comparison of net pressure distributions	50
3.5.4	Comparison of panel-averaged cavity pressures with predicted time-series	55
3.6	Validation of areas considered in the input for the model	58
3.6.1	Sensitivity of the chosen area combination	60
Chapter 4	63
4	Conclusions	63

4.1 Conclusions.....	63
4.2 Future Recommendations	63
References.....	64
Appendix A: Summary of previous research on pressure equalization.....	71
Appendix B: Numerical Method.....	76
Curriculum Vitae	77

List of Tables

Table 3-1: Statistical comparison of results obtained from the analytical model with the spatially averaged time-series obtained from the wind tunnel test.	45
Table 3-2: Sensitivity of predicted results for various combinations of external pressures for 225-degree wind direction	60
Table 3-3: Sensitivity of predicted results for various combinations of external pressures in combination “a” for 225-degree wind direction	62

List of Figures

Figure 1-1: Different types of façade systems: (a) Solar Façade (b) Double-Skin Façade (c) Two high-rise buildings with porous façades. 3

Figure 1-2: Schematic representation of wind loading mechanism on a double-skin, air-permeable façade system. 4

Figure 1-3: Example of double-layer systems (a) Solar panel array on a sloped roof (b) Loose-laid roof pavers 5

Figure 2-1: Flow into and out of a double-layer system with two openings (Oh and Kopp, 2014). 16

Figure 2-2: Simplified idealization of (a) mean flow and (b) pressure distributions on external surface and cavity of panels (Oh and Kopp, 2014)..... 17

Figure 2-3: Flow into and out of a double-layer system with multiple openings 18

Figure 2-4: Schematic representation of a solar panel array system located on the roof of a building 21

Figure 2-5: (a) Schematic representation of shroud around the panel array system to restrict the direct entry of air to the cavity through sides, and (b) edge sealing in double-skin façades, which prevents cavity flow to enter adjacent cavity. 22

Figure 2-6: Schematic representation of flow separation and cavity flow when the wind direction is perpendicular to the face: (a) Isometric view and (b) Sectional view. 24

Figure 2-7: Schematic representation of flow separation and cavity flow when the wind direction is coming at an inclined angle to the roof..... 26

Figure 3-1: Photo of the Boundary Layer Wind Tunnel at the University of Western Ontario along with the study model having solar panels on the sloped roof (Stenabaugh, 2015)..... 29

Figure 3-2: Wind tunnel physical model of the solar panel arrays on the flat roof surrounded by shroud (Stenabaugh (2015))..... 30

Figure 3-3: Drawings of the solar panel array showing the panel dimensions: (a) top view and (b) sectional view (Stenabaugh, 2015).....	31
Figure 3-4: (a) Photos of the solar panel array system and (b) a close-up view of a single panel showing the position of pressure taps on the top surface of the panel (Stenabaugh, 2015).	32
Figure 3-5: The mean pressure distribution for 135 degree wind direction for external and (b) cavity pressures.....	(a) 34
Figure 3-6: The mean pressure distribution for 203 degree wind direction for external and (b) cavity pressures.....	(a) 36
Figure 3-7: The mean pressure distribution for 225 degree wind direction for external and (b) cavity pressures.....	(a) 37
Figure 3-8: The mean pressure distribution for 315 degree wind direction for external and (b) cavity pressures.....	(a) 38
Figure 3-9: Flow chart showing the algorithm of the analytical model.....	40
Figure 3-10: Areas considered for the area-averaged external pressures for various wind directions (a) 135 degree (b) 203 degree (c) 225 degree and (d) 315 degree	42
Figure 3-11: Comparison of time series obtained from analytical model with the experimental results for a wind direction of 135 degrees.....	43
Figure 3-12: Spectra comparison of analytical results with the experimental results for 135 degree wind direction	44
Figure 3-13: Comparison of time series obtained from analytical model with the experimental results for 203-degree wind direction.	46
Figure 3-14: Spectra comparison of analytical results with the experimental results for 203-degree wind direction.....	46

Figure 3-15: Comparison of time series obtained from analytical model with the experimental results for 225-degree wind direction.	47
Figure 3-16: Spectra comparison of analytical results with the experimental results for 225-degree wind direction.....	47
Figure 3-17: Comparison of time series obtained from analytical model with the experimental results for 315-degree wind direction.	48
Figure 3-18: Spectra comparison of analytical results with the experimental results for 315-degree wind direction.....	48
Figure 3-19: Distribution of the external and cavity pressure correlation coefficients from the experimental results	49
Figure 3-20: Distribution of the external and cavity pressure correlation coefficients from the analytical model	50
Figure 3-21: Contour map of net pressure distributions for the 135-degree wind direction for (a) experimental and (b) analytical mean net pressures and for (c) experimental and (d) analytical peak net pressures.....	51
Figure 3-22: Contour map of net pressure distributions for the 203-degree wind direction for (a) experimental and (b) analytical mean net pressures and for (c) experimental and (d) analytical peak net pressures.....	52
Figure 3-23: Contour map of net pressure distributions for the 225-degree wind direction for (a) experimental and (b) analytical mean net pressures and for (c) experimental and (d) analytical peak net pressures.....	53
Figure 3-24: Contour map of net pressure distributions for the 315-degree wind direction for (a) experimental and (b) analytical mean net pressures and for (c) experimental and (d) analytical peak net pressures.....	54

Figure 3-25: Comparison of panel-averaged cavity pressures from the experimental data with the (single) cavity pressure obtained from the analytical model for 135-degree wind direction 55

Figure 3-26: Comparison of panel-averaged cavity pressures from the experimental data with the (single) cavity pressure obtained from the analytical model for 203-degree wind direction 56

Figure 3-27: Comparison of panel-averaged cavity pressures from the experimental data with the (single) cavity pressure obtained from the analytical model for 225-degree wind direction 57

Figure 3-28: Comparison of panel-averaged cavity pressures from the experimental data with the (single) cavity pressure obtained from the analytical model for 315-degree wind direction 58

Figure 3-29: Various combinations of external pressures and areas checked for 225 degree wind direction 59

Figure 3-30: Sensitivity cases considered for combination “a” for 225-degree wind direction. 61

List of Appendices

Appendix A: Summary of previous research on pressure equalization	71
Appendix B: Numerical Method.....	76

Nomenclature

The nomenclature used throughout the thesis is listed below.

k	= the discharge coefficient
\dot{U}	= the temporal-derivative of the velocity through the area of the opening
\overline{V}_h	= the mean velocity at roof height
A	= the tributary area
A_o	= the area of openings
C_L	= orifice loss coefficient
$C_{pe}(t)$	= instantaneous external pressure coefficient
$C_{pi}(t)$	= instantaneous cavity pressure coefficient
G	= the gap between the modules or panels
H	= the depth of the cavity
K_L	= effective steady state loss coefficient
P_{AE}	= area-averaged pressure
$P_e(t)$	= instantaneous external pressure time series
$P_i(t)$	= instantaneous cavity pressure time series
P_o	= the static pressure
a_i	= weighted area for the area-averaged pressure
f_b	= the body force
f_i	= the pipe-friction factor
l_e	= effective length of the fluid passing through the orifice
l_o	= the thickness of the external layer
p	= pressure
u_j	= the velocity component along j direction
u_k	= the velocity component along k direction

ΔP = the differential pressure

μ = the viscosity of the fluid

ρ = density of the fluid (air)

Chapter 1

1 Introduction

Nowadays, the design community is coming up with wide variety of designs for tall buildings and civil structures, which add value to not only the aesthetic looks but also to the overall performance of the buildings in terms of energy consumption and design wind loading. This urge to come up with creative designs has led to the introduction of unique elements in the outer layer, or façade, of buildings and roofs. Some of the new approaches in design are shown in Figure 1.1, which include intelligent facades that react to the outdoor temperature and light and change properties with respect to the outdoor conditions. There are also solar façades, which function as exterior façades as well as generating electricity, double skin facades and porous façades for better aesthetics and performance in energy consumption. But the most important point to be noted here is that the wind-loading mechanism for these new elements are different from those on conventional glass facades, for many reasons. One of the most important discrepancies between these new type of designs and the conventional ones is the presence of a cavity between the outer layer and the inner layer, along with the permeability of the outer layer. A schematic diagram showing the wind loading mechanism on a double-layer façade system is shown in Figure 1.2. The figure indicates that the outer surface of the external layer is exposed to wind, which causes a time-varying surface pressure distribution. At the gaps, the external pressures are (partially) transmitted through the opening, such that there is airflow in the cavity, causing a time-varying pressure distribution on the interior surfaces. For many cladding systems, such as rain screen walls, the design intent is to have as little load as possible on the external layer, Depending on the geometry of the openings and cladding system, the cavity pressure can become relatively close to the external pressure, which leads to low net wind loads. This process is called pressure equalization (or, sometimes, pressure moderation).

1.1 Background

In conventional buildings, a proper understanding of wind-induced pressures on the outer layer of the building is enough for the design of the façade elements. But in buildings with double skin façades or multi-layer systems, as shown in Figure 1.1, the outer layer can be porous or have gaps between the layers such that the wind-induced external pressures can be transferred to the cavity between the layers. So, for the design of these systems, it is important to know the mechanisms of overall net wind loading on the external layer, as well as the cavity pressure. The mechanism of transfer of external pressure to the cavity, and, thereby, equalizing the external and cavity pressure, is known as pressure equalization. Significant pressure equalization occurs when the external or outer flow pressure is transmitted to the underside of a layer through the openings. Normally the term pressure equalization is used in the case of cladding components with openings, as it denotes a tendency to decrease the net wind load, which is the overall effect of external and cavity pressures.



(a)



(b)



(c)

Figure 1-1: Different types of façade systems: (a) Solar Façade (b) Double-Skin Façade (c) Two high-rise buildings with porous façades.

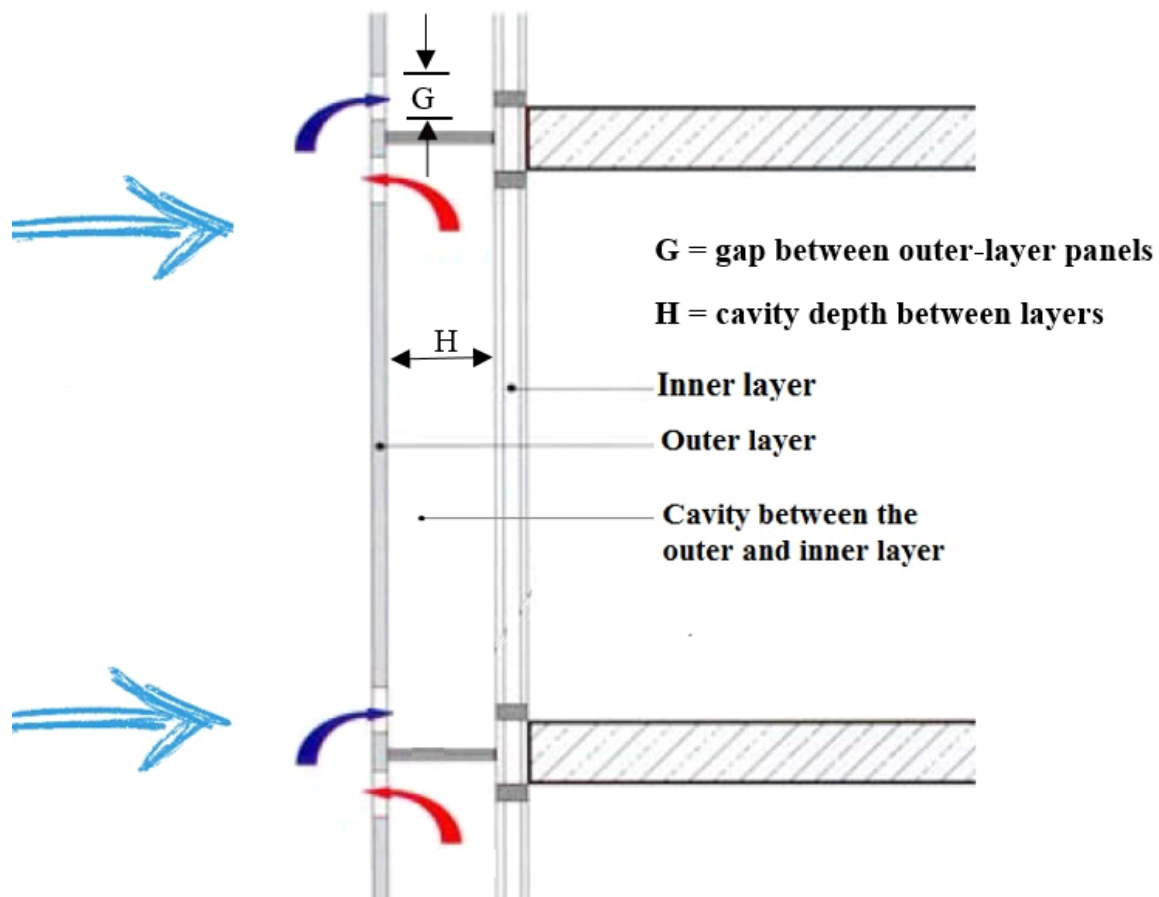


Figure 1-2: Schematic representation of wind loading mechanism on a double-skin, air-permeable façade system.

Some practical examples in which the mechanism of pressure equalization occurs are solar panel array systems in roof and loose-laid roof pavers, shown in Figure 1.3, along with the systems shown in Figure 1.1. In all these systems, there is an external layer with openings and an internal layer separated by a cavity. Hence, the external layer gets pressurized from both sides and pressure equalization plays a major role in these systems. In the following sections, the literature regarding wind loads on such systems is examined, with a summary of all relevant papers provided in Appendix A in tabular form.



**Figure 1-3: Example of double-layer systems (a) Solar panel array on a sloped roof
(b) Loose-laid roof pavers**

1.2 Analytical models in literature

The initial attempts to develop an analytical model for pressure equalization were by Killip and Cheetham, (1984); Fazio and Kontopidis, (1988); Baskaran and Brown, (1992); Xie et al, (1992) which used the discharge equation for flow through openings with the assumption of incompressible flow. Burgess (1995) and Van Schijndel and Schols (1998) developed analytical models using the discharge equation for flow through openings and the ideal gas law.

Inculet and Davenport (1994), Choi and Wang (1998), and Kumar and Van Schijndel (1999) introduced unsteadiness by using the unsteady discharge equation, i.e., the Helmholtz resonator model of Holmes, (1979) and Vickery, (1986), and the predicted net pressures on the outer layer. These models were observed to match the experimental data well. However, the models were limited to the particular condition of spatially uniform external pressure, i.e., a single external pressure. To model cavity pressures that are spatially varying because of longitudinal flow in the cavity, Amano et al. (1988), Trung et al. (2010) and Lou et al. (2012) also used Helmholtz resonator model from Holmes, (1979) and Vickery, (1986).

The discharge equation has been widely employed in wind engineering to model the flow through an opening by Holmes (1979), Vickery (1986), Sharma and Richards (1997), Oh et al. (2007), Kopp et al. (2008) and Ginger et al. (2010). However, it may not be sufficient to describe fluid motion in the cavity because there should be significant

viscous effects involved in the cavity flow, in particular, in the case of a cavity, which is thin and long. Sun and Bienkiewicz (1993) developed an analytical model to estimate the pressure distributions in the cavity underneath loose-laid roof pavers with the assumption of steady flows in gap and cavity and, hence, Darcy's law was used to model the mean flow. But this model is applicable only for flow at low Reynolds Number.

For conventional buildings, the proper estimation of wind-induced pressures on the external façade or net pressures across elements like canopies or parapets, which are exposed to wind on both sides can be easily done using conventional wind tunnel test. But in the case of multi-layer systems having gaps/porosity in the external layer and a cavity between external and inner layer, the estimation of wind loading across the external layer or in the inner layer can be quite difficult for many practical reasons. Mainly, conventional wind tunnel tests are conducted at a range of model scales from 1:200 to 1:400 and in that range of model scales, it is practically impossible to model the gap between the outer and inner layers as they will be very small in magnitude. As well, the wind tunnel tests model, the volume of the cavity can be different from the real case due to the PVC tubes that are used to connect the pressure sensors with the scanner, which can create significant blockage and resistance to the flow in the cavity, changing the flow characteristics and pressure distribution.

So, the prediction of cavity pressures by analytical models is a worthwhile endeavor and there has been significant previous research that deals with the mechanisms of pressure equalization and estimation of wind-induced pressures on roof mounted solar panel systems or other such multi-layer systems.

But the problem has not been completely resolved and there is still a lack of accurate models for the estimation of cavity pressure in multi-layer systems. Even the current codes/standards don't provide guidance for the design of multi-layer systems, apart from ASCE 7-10 which suggest a reduction factor for the design of porous cladding only if the test data or literature approve lower loads. Some of the findings from the studies mentioned earlier have begun to appear in NEN 7250 (2013) and SEAOC PV2-2012 (2012). Many of the analytical models that are developed in the past were focused on

modeling and estimating the cavity pressure within the compartment, whereas there has been less attention towards the variation of cavity pressures, spatially and temporally. It is important to know the influence of porosity of the external layer on the cavity pressure for suggesting realistic design loads. With this vision, a new approach has been used to estimate the cavity pressures in air-permeable, multi-layered systems and the results are validated with experimental results from Stenabaugh (2015).

1.3 Previous studies on loose-laid pavers

Some of the most important research related to the mechanisms of pressure equalization were carried out for loose-laid paver systems on flat roofs, which analyzed the effect of gaps between the modules as well as the impact of cavity depth. Kind and Wardlaw (1982) conducted failure model studies on loose-laid roof pavers to understand the lifting and overturning of roof-mounted pavers. The results showed that the net wind loading on the outer layer of the roof system (i.e., the pavers) was much lower than the pressure values on a normal roof due to pressure equalization between the upper and lower surface of the roof pavers. In other words, introducing gaps in between the roof pavers can reduce the chances of failure or blow-off of roof pavers. Based on the results from the failure model tests, a correlation model was developed by Kind et al. (1988) for predicting the wind speeds causing failure of roof pavers. Okada and Okabe (1991) analyzed the effect of height of cavity beneath the roof pavers by conducting failure tests at different heights and found that too much height can have a reverse impact on pressure equalization and can lead to failure of roof pavers.

Bienkiewicz and Sun (1992, 1997) experimentally studied the pressures, especially the cavity pressures beneath the scaled paver systems on the flat roof of a low-rise building for a cornering wind direction, and found that even a small cavity beneath the panels can significantly reduce the peak and mean cavity pressures and that the cavity pressures can be more of uniform for relatively larger cavity depths. The change in net loading due to the introduction of flow resistance in the cavity were also analyzed. These authors concluded that both the paver size and aspect ratio play a major role in the wind resistance of the roof pavers systems.

Sun and Bienkiewicz (1993) developed an analytical model to estimate the pressure distributions in the cavities below the loose-laid roof pavers. The model was developed based on the assumption that the flow through the gaps as well as the cavities are steady flow and, hence, Darcy's law was used to model the mean flow. However, the model can be used only for small crack-like openings where the Reynold's number of the flow is very small.

Holmes (2007) also did similar studies for cornering winds and investigated the mechanism behind loading on roof pavers due to flow separation and re-attachment caused due to the rotation of vortices, when the wind is along the corner of the roof. Bienkiewicz and Endo (2009) did similar studies as Bienkiewicz and Sun (1992, 1997) by accounting for the effects of gaps on the overall loading on roof paver systems. The results showed that overall loading on the pavers depend on the permeability of the outer layers and the flow resistance in the cavity and that the wind uplift can be significantly reduced by increasing the gaps (permeability) in the outer layers. The reduction in the uplift of the pavers for different values of the permeability of outer layers was also quantified. The effect of ratio of gap (G) between the outer layer and the inner layer and the depth of the cavity (H) was examined in large-scale tests conducted at Wall of Wind by Asghari Mooneghi et al. (2014) and concluded that increasing the G/H ratio can lead to reduced net loading on these systems.

1.4 Previous studies on roof-mounted solar panels

Pressure equalization plays a vital role in the wind design of roof-mounted solar panel array systems. The pressure in the cavity between the solar panel module and the roof had to be approximately equivalent to the pressure on the external or upper surface of the panel to achieve appropriate pressure equalization and thereby reducing the net loads on the solar panel modules. Proper understanding about the wind loading mechanism on the solar panels modules are extremely important as it may affect the overall cost and also the lifespan of the solar panel array systems.

There have been many studies which examined the various factors which affect the wind loading and also the mechanism of pressure equalization on the solar panel arrays

(Pratt and Kopp, 2013; Kopp et al., 2012; Kopp and Banks, 2013; Geurts and van Bentum 2006, 2007; Banks, 2013; Banks et al., 2000; Cao et al., 2013). Pratt and Kopp (2013) have shown that building size plays a significant role in the wind loads on tilted solar panel arrays mounted on building roofs, as the size of the vortices generated on the roof are controlled by the building size. This was reconfirmed by Kopp et al. (2012) and Banks (2013) who showed that this was due to the formation of corner vortices since the corner vortices are strengthened by vortex stretching and continuous separation along the building walls. Kopp et al. (2012) also confirmed that the forces acting on the solar panel array mounted on a building roof can be complex since the wind field is influenced not only by the natural turbulence of the wind but also from vortices and separation along building edges. The strength of the vortex created directly controls the magnitude of suctions on the roof (Kind, 1986). Banks et al. (2000) found that the position of largest peak suctions on the roof was between the vortex core and the reattachment line on the roof. Kopp (2013) found out that the estimation of aerodynamic forces, especially the uplift, is pivotal for the design of tilted solar panel arrays installed on flat roofs of low-rise buildings since they control the required counter force to resist the uplift of panels. Banks (2013) showed through his research that the wind loads are sensitive to the direction of panel tilt and swirl direction of the corner vortex for solar panel installations on building roof and hence using the existing literature for the design of panel arrays installed on building roof has to be done with extreme caution especially when the panel array rows are not aligned with building edges. In addition to the above results, Browne et al. (2013) also reviewed the impact of parapets on wind loading on solar panel arrays on building roofs and found that the corner vortices can increase the loads when there are parapets around the panel arrays.

The role of array geometry on wind loads was studied by Kopp et al. (2012) and they found that loading mechanisms on solar panel arrays were different depending on the tilt angle of the modules and also showed that larger modules were associated with an increase in the wind loads for the higher tilt models whereas the module dimensions had much less impact on the lower tilt systems. The study also showed that wind loads on low-tilt arrays were governed by pressure equalization across the modules from the building generated (roof) pressures, whereas the higher tilt arrays were significantly influenced by array-generated flow, which can increase the loads due to weakened pressure equalization.

Kopp (2013) found that both the row spacing and the minimum height above the roof surface (when kept below a particular height) had limited impact on the net wind loads.

The applicability of roof zones in current design standards were studied by Banks (2013) and Kopp (2013). Since it is obvious that the wind loading on panel arrays is different than that on bare roof loads, there have been some recent studies that focused on the applicability of current design codes/standards for designing solar panel arrays on the roof, especially the applicability of roof zones in these systems. In addition to this, Kopp (2013) reported that edge roof zones for solar panel designs should be larger, i.e., about 50-60% of H for lower tilt angles and 80% of H for higher tilt angles, which will account for the different locations of peak uplift in the panel arrays. The fact that the aerodynamics of solar panel systems are different from conventional flat roofs was further confirmed by Pratt and Kopp (2013) by simultaneous pressure measurements and particle image velocimetry (PIV) which measured the flow field in an experiment and the results showed that the largest uplift on solar panels are caused by the vertical velocity component in the vortex which was created due to the separation of flow at the building edge.

Ginger et al. (2011), Stenabaugh et al. (2010, 2011) and Geurts and Blackmore (2013) studied the wind loading and pressure equalization on solar modules mounted parallel to roofs. Ginger et al. (2011) studied the wind loads on solar panel arrays on gable roofs with different slopes from 7.5 degrees to 22.5 degrees and developed design guidelines. The position of arrays on gable roofs was changed for each configuration and that effect was also analyzed. The results showed that H did not have a significant impact over the results. However, it is critical to note that the arrays were modeled with no gaps between the panels and hence the whole array was considered as a single large panel. A similar study was done by Stenabaugh et al. (2010, 2011) in which a single solid panel was used to represent the whole panel array and the results indicated that the net loads were close to the external pressure coefficients on bare roof. The impact of changing the position of the panels were also studied and found that when the panel arrays are located at the ridge, the uplift forces could be increased due to the positive pressure acting on the underside of the panels located near the ridge. Aly and Bitsuamlak (2014) also reported

similar results from the studies conducted on solar panel modules mounted parallel to a sloped gable roof system.

Another study conducted on solar panel arrays modeled as a single unit was done by Geurts and Blackmore (2013) in which both full-scale and model scale tests were conducted on a hip roof. Eventhough this study considered a single module with no gaps like Stenabaugh et al. (2010, 2011) and Ginger et al. (2011), the module was considerably smaller. The results showed that the external peak pressures on the upper side of the panel are higher for large H, whereas on the underside of the panel, peak positive pressures were found to be increasing with increase in H and peak suctions were smaller. The results confirmed that there was significant correlation between external and cavity pressures but the intensity of pressure equalization was different from Stenabaugh et al. (2010, 2011) and Ginger et al. (2011), as the modules used in their studies were much larger in size. Stenabaugh et al. (2015) studied the effect of G and H on the wind loading on photovoltaic panel arrays and found that larger G along with smaller H will yield low net loads on panels and a pressure equalization factor was also evaluated using the peak minima as a function of tributary areas of panels.

1.5 Previous studies on porous and rainscreen systems

Some of the most notable studies on wind loading on porous cladding systems were by Gerhardt and Kramer (1983), Cheung and Melbourne (1988), Gerhardt and Janser (1994), Richardson and Richards (1995), Lee and Kim (1998), Richardson and Richards (1999), Briassoulis et al. (2010) and Cope et al. (2013).

One of the most important early experimental investigations on the wind loading on porous cladding systems was carried out by Gerhardt and Kramer (1983), whose results showed that increasing the permeability of cladding systems or increasing the resistance of cavity flow can decrease the net wind pressures across the porous layer. Cheung and Melbourne (1988) studied the effects of porosity and internal volume on the mean, standard deviation and peak pressures on a porous surface and reduction factors were suggested so that design wind loads on porous cladding can be estimated from external pressure coefficients in codes.

Gerhardt and Janser (1994) extended their previous work and studied the impact of parameters like relative building dimensions, porosity and gap width and the results were validated, to some extent, with full-scale measurements. The results showed that the internal pressure in the gap followed the external pressure qualitatively for small gaps, but was almost independent of building “height” or “dimensions” for large gap widths. The net wind pressure coefficient across the outer permeable skin was highest when the gap was large and increased permeability of the outer layer reduced the net wind pressure coefficient and moreover edge sealing, i.e., the vertical edges of the buildings are closed, which prevents the wind to flow from one façade to another, helps to reduce the net wind load across the permeable outer layer.

Richardson and Richards (1995) conducted full-scale measurements of porous wind break and the response of porous structures at different frequencies were analyzed. The study was further extended by Richardson and Richards (1999) to understand the relation between porosity and loss coefficient and their impact on wind loading and found that for round wire mesh screens, the loss coefficient is related to the porosity and for other structures the loss coefficient depends on the porosity and the construction. The shelter effect of a porous wind fence on a triangular prism was experimentally simulated in a circulating water channel by Lee and Kim (1998) and results showed that the fence decreases the turbulent intensity and turbulent kinetic energy around the prism, especially at the top of prism model, turbulent kinetic energy is about half of that without the fence. Lee and Park (1998) extended their previous research and found that a porous fence with porosity of 40-50% is most effective for the reduction of pressure fluctuations on the model surface and the mean pressure coefficients decreased when the fence height is greater than the model height.

Some of the most important research about the design wind loading and the pressure equalization mechanism in rainscreen systems were conducted by Killip and Cheetham (1984); Pazio and Kontopidis (1988); Baskaran and Brown (1992); Incullet and Davenport (1994); Burgees (1995); Kumar and van Schijndel (1999); Kumar and Wisse (2001); Kumar et al. (2003). Killip et al. (1984) studied the mechanism of rain penetration through walls and joints and a theory about the functioning of the pressure equalizing rain-screen

wall was suggested, which recommended the methods to improve the effectiveness of pressure equalization in the cavities of rainscreen systems. Pazio and Kontopidis (1988) investigated the correlation among cavity pressure, wind pressure and openings and the results showed that the cavity pressure is equal to the average of wind pressure around the building where the outer layer has only cracks and no vent hole and the cavity pressure is not equal to average for uniformly distributed openings on outer layer. Baskaran and Brown (1992) developed an analytical model to simulate Pressure Equalized Rainscreen (PER) wall performance and also conducted full-scale field measurements as well as laboratory tests to compare the results, which showed that venting area of at least 1% of the wall area is necessary for pressure equalization in cavities. The results from Baskaran and Brown (1992) were also compared with the numerical model created using Computational Fluid Dynamics (CFD) by Baskaran (1994).

Inculet and Davenport (1994) analyzed the impact of venting area, air barrier leakage, cavity volume and compartment size in pressure equalization of rainscreen walls and concluded that an increase in venting area for constant volume or a decrease in volume for constant venting area results in both a higher natural frequency and a higher critical damping frequency. Burgees (1995) studied the effect of geometric alterations i.e. joint opening area and joint cavity volume in pressure equalization and suggested that 100% air pressure equalization can be achieved purely through geometric alteration of the dimensions of pressure equalized, rainscreened joints. Kumar and van Schijndel (1999) developed two theoretical models, one based on mass balance and the other based on Helmholtz resonant theory to understand the influence of various design parameters on pressure equalization and the results showed that the model based on mass balance was sufficiently accurate to predict the pressure equalization and the results were also compared with the full scale data. Kumar and Wisse (2001) did frequency domain analysis to understand the technicalities of the pressure equalization in rainscreen facades and the results were matching with the previous studies. Kumar et al. (2003) did full-scale measurements on rainscreen walls and the results were used to highlight the shortfalls of codes/standards in addressing the loads for rainscreen facades. Previous studies on areas related to pressure equalization and their relevant theoretical and experimental studies have been summarized in Appendix A along with their contributions.

1.6 Objective of the thesis

Air-permeable multi-layer systems are becoming more popular as an integral part of buildings. These systems can be in the form of solar panel arrays on the roof of the building, double-skin facades or as loose-laid roof paver systems. In all these systems, which have an air-permeable external layer along with a cavity between the external and internal layer, the determination of wind loads on the inner cavity or across the external layer, by experimental method like wind tunnel test, is not possible due to practical reasons. From the literature survey explained above, it is clear that there has been a lot of studies which focused on the effect of opening size and the impact of cavity depth and other factors which controls the pressure equalization in these systems. But an accurate, practical, analytical model which can address the issues completely is still lacking.

The objective of this study is to do a proof-of-concept work to make sure that the lumped-leakage approach can be used to estimate the time-varying cavity pressure distributions in a double-layer system with an air-permeable outer layer, given the external pressure on the outer surface. As a part of this work, a framework for an analytical model that can estimate the cavity pressure will be suggested. The model uses orifice discharge equation and conservation of mass equation as governing equations and the results from the analytical model are compared with wind tunnel results of a solar panel array study obtained from Stenabaugh (2015).

Chapter 2

2 Analytical modeling for the estimation of cavity pressure

2.1 Introduction

In this chapter, an analytical model for the estimation of cavity pressure in an air-permeable double-layer system is modelled. The governing equations of the analytical model were derived from the general equation for orifice flow. The model uses the time histories obtained from the pressure taps located on the external surface of the system as input, along with the geometric parameters of the multi-layer cavity system, to estimate time histories of cavity pressures.

2.2 Mathematical Formulation

The general equation for flow through an orifice can be derived from the Navier-Stokes equation, as shown in Oh and Kopp (2014). The assumptions considered in the derivation and other parameters accounted in the mathematical derivation are explained below.

2.2.1 Equations for flow through an orifice

The equation for fluid flow through an orifice can be derived from the Navier-Stokes equation for incompressible flows,

$$\rho \frac{\partial u_j}{\partial t} + \rho u_k \frac{\partial u_j}{\partial x_k} = -\frac{\partial p}{\partial x_j} + \mu \frac{\partial^2 u_j}{\partial x_j \partial x_j} + \rho f_{bj} \quad (2.1)$$

where ρ is the density of the fluid, u_j is the velocity component along j direction, u_k is the velocity component along k direction, p is the pressure, μ is the viscosity of the fluid and f_b is the body force.

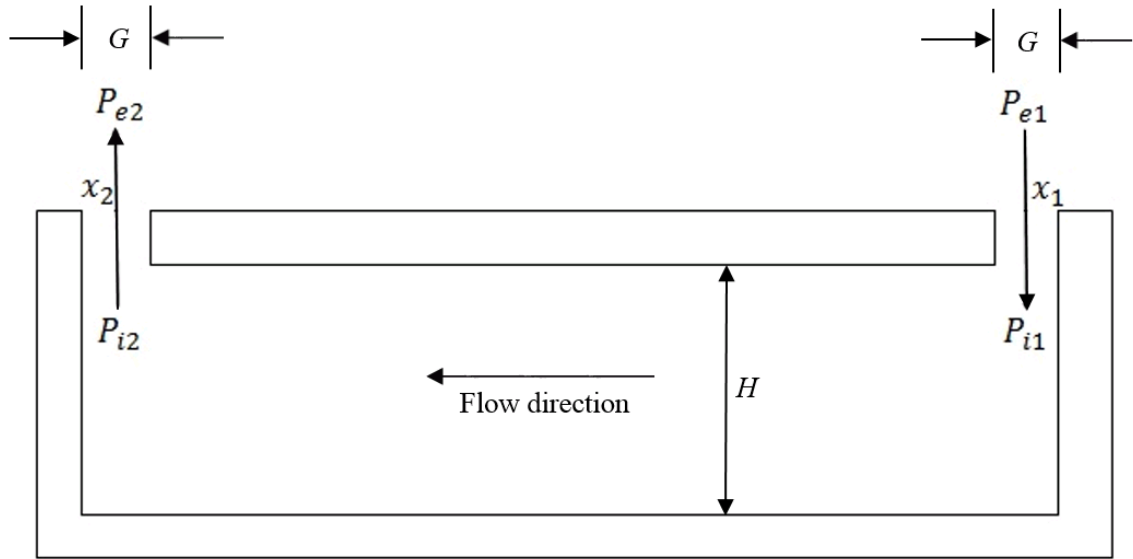


Figure 2-1: Flow into and out of a double-layer system with two openings (Oh and Kopp, 2014).

Oh and Kopp (2014) and Oh (2014) showed that Eq. 2.1, when applied to the system shown in Figure 2.1, becomes

$$\rho l_e \dot{U} + C_L \frac{\rho}{2} U|U| + \frac{12\mu l_o}{G^2} U = \Delta P \quad (2.2)$$

where l_e is the “effective length” of the fluid passing through the orifice, \dot{U} is the temporal-derivative of the velocity through the area of the opening, which is $\frac{dU}{dt}$ and is assumed to be constant, C_L is a loss coefficient, l_o is the thickness of the external layer, G is the width of the opening, i.e., the orifice, and ΔP is the differential pressure which is the difference in external pressures at locations x_1 and x_2 i.e. Pe_1 and Pe_2 , as shown in Figure 2.1. The arrows in the figure indicate the direction of flow for $Pe_1 > Pe_2$. It is also assumed that there is no vertical pressure gradient such that there is a single value for the pressure at each horizontal location.

A similar approach has been used by Holmes (1979), Vickery (1986) and Oh et al. (2007) to estimate the internal pressures within buildings. In such cases, where there is a single opening into a sealed room or building, the continuity equation was used along with

the unsteady discharge equation, (Eq. (2.2)), which provides two unknowns, i.e., the velocity of flow through the opening and the internal pressure.

2.2.2 Concept of neutral pressure line

Oh and Kopp (2014, 2015) studied the mechanism of pressure equalization and suggested the concept of neutral pressure line. Consider a panel array as shown in Figure 2.2 (a), with five openings and the flow entering and leaving the cavity are also shown using arrows. The idealization of mean flow and pressure distribution mechanisms on external surface and interior cavity are shown in Figure 2.2 (b).

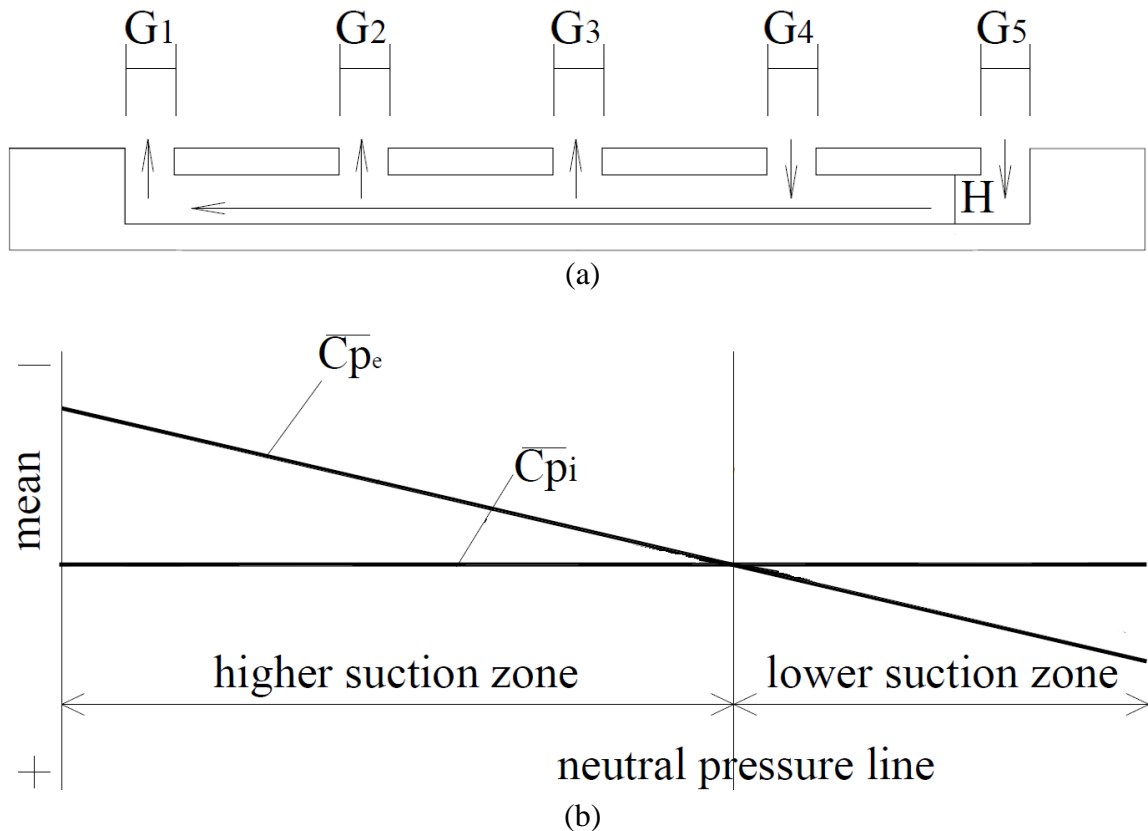


Figure 2-2: Simplified idealization of (a) mean flow and (b) pressure distributions on external surface and cavity of panels (Oh and Kopp, 2014)

In these plots, the pressure distributions are idealized for simplification and to better explain the mechanism. As a part of this simplification, the distribution of mean external pressure coefficient is depicted as a solid straight line and if the G/H ratio is small, the

mean cavity pressure coefficients are more uniform. This leads to the formation of three different pressure zones in the panels depending on the gradients of mean external coefficient of pressure, \bar{C}_{pe} and mean cavity coefficient of pressure, \bar{C}_{pi} . The regions in which $\bar{C}_{pe} < \bar{C}_{pi}$, there will be higher suction zones, i.e., the mean upward pressures will be higher and in regions where $\bar{C}_{pe} > \bar{C}_{pi}$, the mean downward pressures will be higher resulting in lower suction zones. At $\bar{C}_{pe} = \bar{C}_{pi}$, there will be zero pressures and this region is called as neutral pressure line. The flow through the gaps are generated due to the difference of external pressures between the gaps.

2.2.3 Equations for flow through multiple openings

Consider a one-dimensional flow in a cavity with multiple openings, as shown in Figure 2.3. In this case, there are five openings and, hence, there will be five discharge equations, one for the flow through each opening (orifice). Here it is assumed that the flow is entering the cavity through openings x_1, x_2 and x_3 and the flow is leaving the cavity through openings x_4 and x_5 , as indicated by the directions of the arrows.

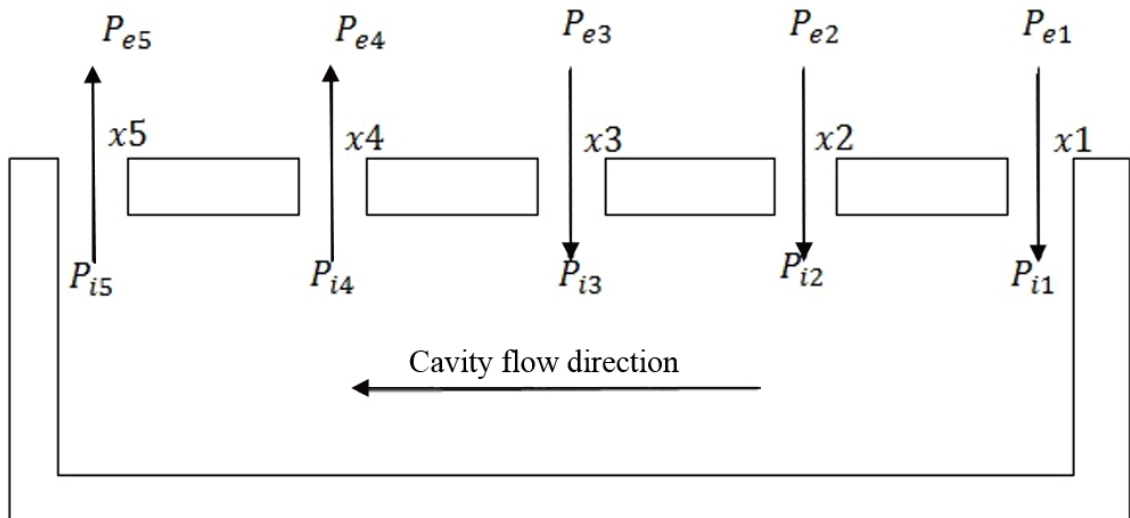


Figure 2-3: Flow into and out of a double-layer system with multiple openings

In other words, by applying Eq. 2.2 for the double layer system shown in Figure 2.2 for multiple openings, one obtains

$$\rho l_{e1} \dot{U}_{g1}(t) + C_{L1} \frac{\rho}{2} U_{g1}(t) |U_{g1}(t)| + \frac{12\mu l_{o1}}{G_1^2} U_{g1}(t) = P_{e1}(t) - P_{i1}(t) \quad (2.3)$$

$$\rho l_{e2} \dot{U}_{g2}(t) + C_{L2} \frac{\rho}{2} U_{g2}(t) |U_{g2}(t)| + \frac{12\mu l_{o2}}{G_2^2} U_{g2}(t) = P_{e2}(t) - P_{i2}(t) \quad (2.4)$$

$$\rho l_{e3} \dot{U}_{g3}(t) + C_{L3} \frac{\rho}{2} U_{g3}(t) |U_{g3}(t)| + \frac{12\mu l_{o3}}{G_3^2} U_{g3}(t) = P_{e3}(t) - P_{i3}(t) \quad (2.5)$$

$$\rho l_{e4} \dot{U}_{g4}(t) + C_{L4} \frac{\rho}{2} U_{g4}(t) |U_{g4}(t)| + \frac{12\mu l_{o4}}{G_4^2} U_{g4}(t) = P_{e4}(t) - P_{i4}(t) \quad (2.6)$$

$$\rho l_{e5} \dot{U}_{g5}(t) + C_{L5} \frac{\rho}{2} U_{g5}(t) |U_{g5}(t)| + \frac{12\mu l_{o5}}{G_5^2} U_{g5}(t) = P_{e5}(t) - P_{i5}(t) \quad (2.7)$$

The velocity at each opening in the outer layer is referred as $U_g(t)$ whereas $P_e(t)$ and $P_i(t)$ refer to the external pressure and cavity pressure, respectively. The numbers in the subscripts (i.e., 1, 2, 3, 4, and 5) denote the location of the gaps, as depicted in Figure 2.2. In order to solve this set of equations, equations representing the conservation of mass are also used.

Employing conservation of mass for the system shown in Figure 2-2, the flow rate entering the cavity should be equal to the flow rate leaving the cavity, i.e.,

$$Q_1 + Q_2 + Q_3 = Q_4 + Q_5 \quad (2.8)$$

where Q is the flow rate through the area of the opening, which gives

$$A_1 \cdot U_{g1} + A_2 \cdot U_{g2} + A_3 \cdot U_{g3} = A_4 \cdot U_{g4} + A_5 \cdot U_{g5} \quad (2.9)$$

where A is the area of the opening.

It should be noted that in general, the flow direction through each opening is unknown until the values for P_{i1} , P_{i2} , P_{i3} , P_{i4} and P_{i5} are established. Thus, the velocity

through the opening is set by its sign. To keep the direction of the losses correct, the form of the loss term is set, as given in the equations.

To date, this kind of approach has only been applied for simulating the one-dimensional cavity pressure distributions due to orifice-type flows through openings, as shown in Oh and Kopp (2014) and Oh (2014). The equations as shown above, cannot be used directly for systems with double layers, such as that as shown in Figure 2.3, without some significant new assumptions and approximations. In double-layer systems such as solar panel arrays located on roofs of buildings, there are gaps (G) between the panel arrays in both directions and the panels are placed at a height (H) above the roof. The openings or gaps between the panels are spread across the whole panel array system and the equations 2.3 to 2.7 have not been previously applied, for estimating the cavity pressures. However, it should be noted that Sun and Bienkiewicz (1993) applied the steady form of these equations to estimate the mean cavity pressure distribution for a roof paver system. (Here, the objective is to establish an unsteady solution.)

Consider the double-layer system shown in Figure 2.3. One of the primary challenges is that the entry points of flow into the cavity below the panels and the exit locations for the cavity flows, which depend on the external pressure distribution, are unknown. In addition to that, a single value for the loss coefficient was used for the original equations. This may not be a practically feasible solution for all scenarios in double-layer systems. Hence, an approach for estimating the cavity pressure in situations where the cavity pressure is uniform is to be developed herein, which utilizes the external pressure distribution, as well as the geometrical parameters, as input parameters. The current analytical model is developed with certain assumptions, which are explained below.

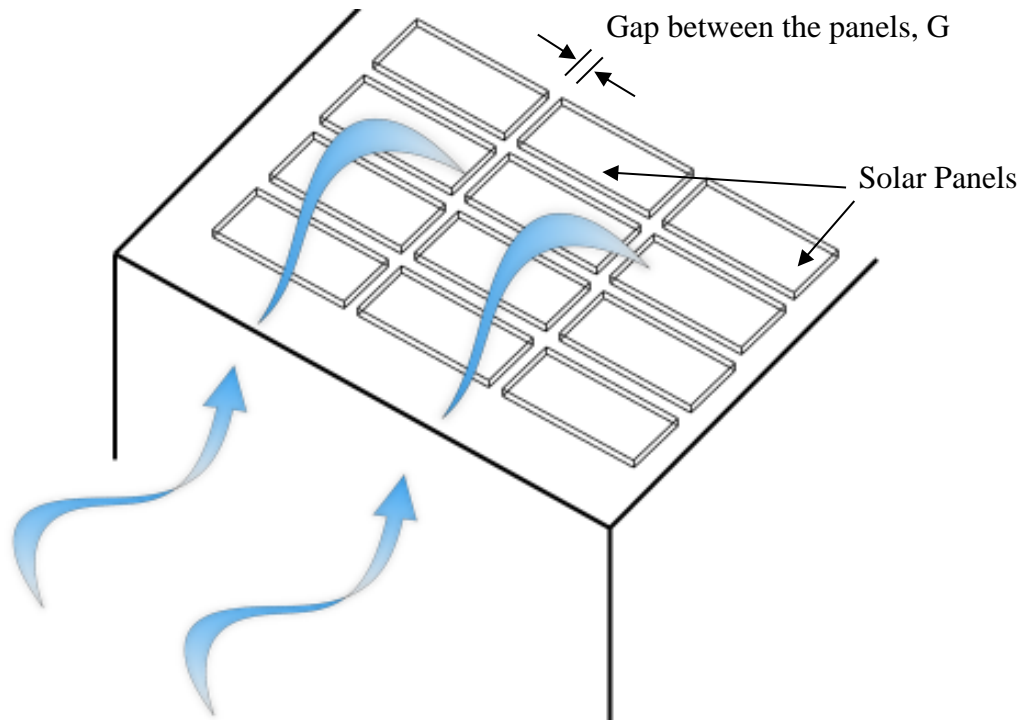
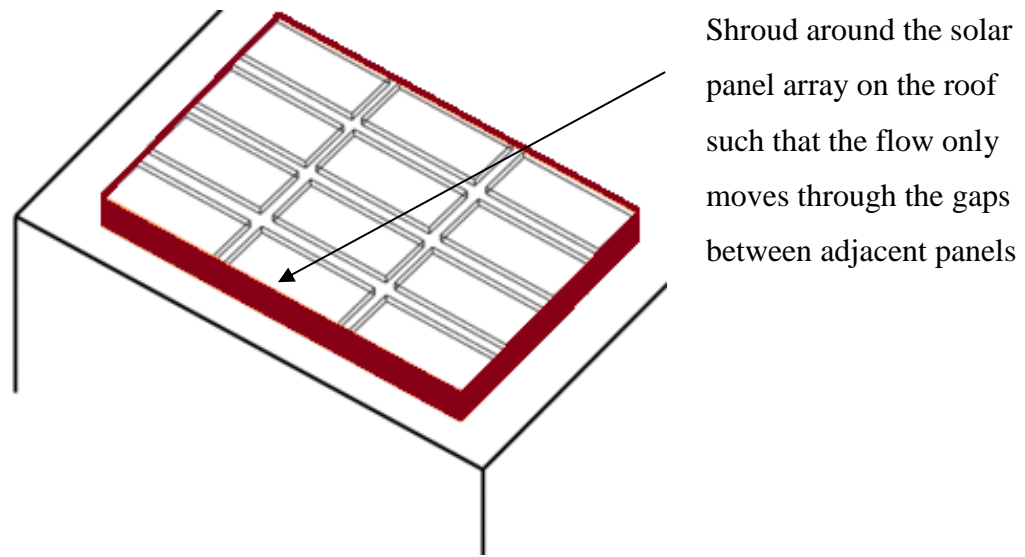


Figure 2-4: Schematic representation of a solar panel array system located on the roof of a building

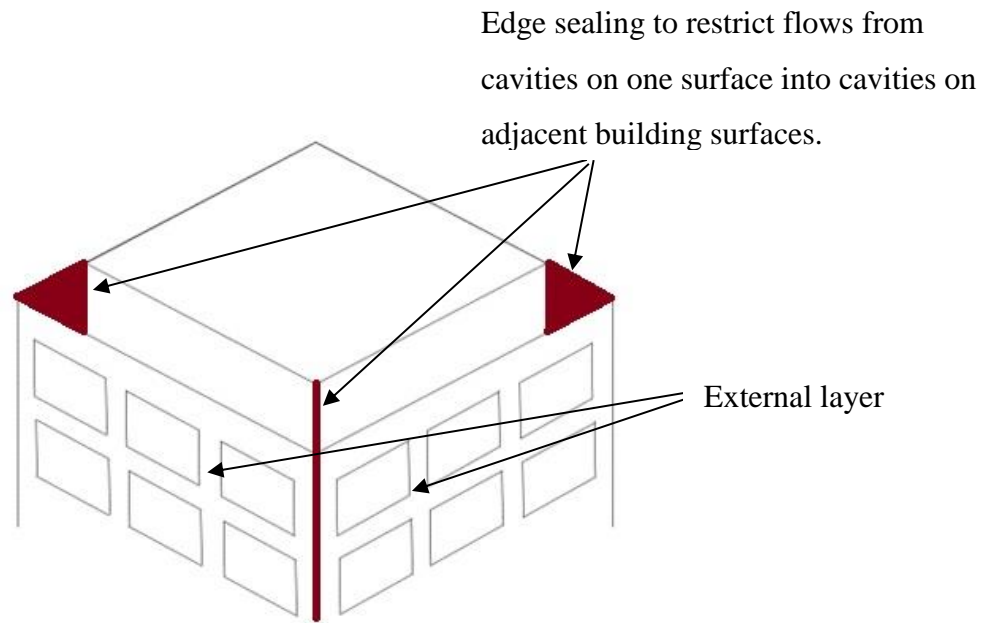
2.2.4 Assumptions considered in the proposed analytical model

The basic assumptions mentioned with respect to Eq. (2.2) remain with the current approach, except for a few modifications. Before getting into the changes to the basic equation, it is important to understand these assumptions:

1. For a double-layer system, as shown in Figure 2.3, the flow can enter or leave the cavity through any openings between the panels or through the gaps between the panels and the roof surface at the edge of the array. In the current model, it will be assumed that the flow can enter or leave the cavity only through the openings in the external layer such that all other openings in the system are closed. In the case of a solar panel array, all other edges are closed by a shroud as shown in Figure 2.4 (a). Similarly, in the case of a double-layer system on a façade, there should be complete edge sealing, which restricts the entry of flow from one cavity to another cavity on the adjacent façade, as shown in Figure 2.4 (b). In both these cases, this ensures that the cavity volume is well-defined.



(a)



(b)

Figure 2-5: (a) Schematic representation of shroud around the panel array system to restrict the direct entry of air to the cavity through sides, and (b) edge sealing in double-skin façades, which prevents cavity flow to enter adjacent cavity.

2. The second important assumption is regarding the cavity pressure. From section 2.2.2, it is clear that the basic equations mentioned in Eq. (2.3) through (2.7) can be used to estimate the spatial variations of cavity pressure values depending on the number of openings. From Oh and Kopp (2015) it is obvious that for small gap to height ratios (G/H), pressure equalization is less effective and the cavity pressure is uniform. In the current model, the cavity pressure is assumed to be uniform, i.e., the effective G/H ratio must be small. This has a significant influence on the approach to solving the equations.

2.2.5 Analytical model for estimating the cavity pressure using a lumped-leakage approach

From the assumptions mentioned in Section 2.2.3 above, consider that for the solar panel array system shown in Figure 2.5, the cavity pressure is approximately uniform and flow can enter or leave the cavity only through the openings between the panels. As well, the solar panel modules in this array are placed at equal distances from each other and the distance between the panels and the roof surface are also kept constant, i.e., the G and H values are constant and uniform.

It is well-known that when wind reaches a building, the flow is separated at edges, creating large vortices and large pressure gradients on the external surface. Normally, the windward edge of the roof has high suction, caused by separated and accelerated flow, which reduce as the flow reattaches. Due to the difference in pressure over the external surface, flow may enter the cavity and the gradient in external pressure distribution determines the entry and exit points for the flow through the cavity. For example, as shown in Figure 2.6, the flow in to the cavity may enter through all the openings in the external surface of region '1' while the flow out of the cavity may come through all the openings in the external surface of the region '2'. The location of the reference (red) line in the figure depends upon the distribution of external pressures, which Oh and Kopp (2014, 2015) called the neutral pressure line, as mentioned in section 2.2.2.

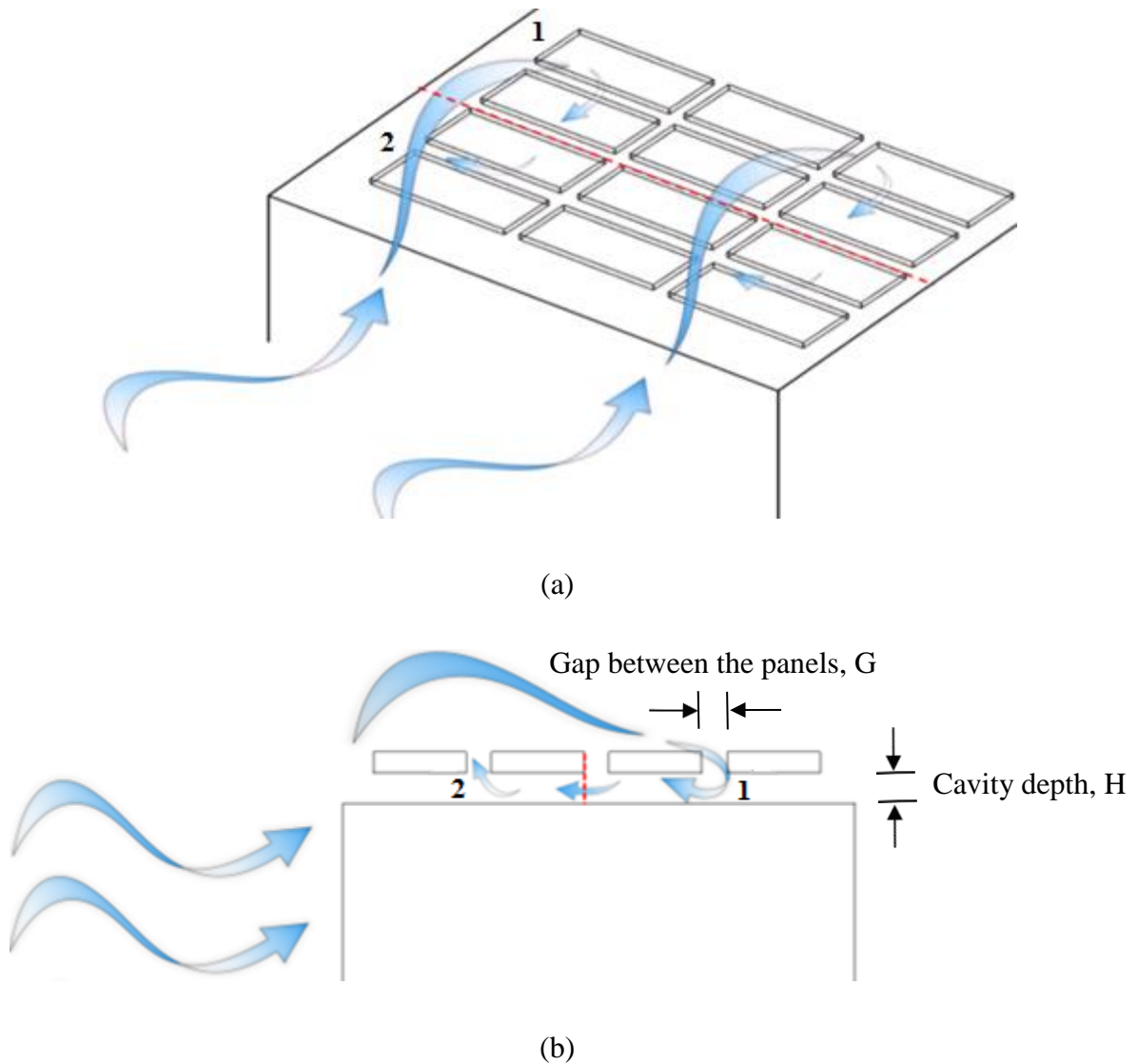


Figure 2-6: Schematic representation of flow separation and cavity flow when the wind direction is perpendicular to the face: (a) Isometric view and (b) Sectional view.

Moreover, if the flow is entering the cavity through all openings in Region '1', then the external pressure distribution over the entire region '1' may be accounted for in the original equation, Eq. (2.2). So, instead of using the individual $P_e(t)$ values, an area-averaged external pressure value is given as input to the analytical model. The area-averaged value of the pressure in region 1 will be called P_{AE1} and area-averaged value of

the pressure in region 2 will be P_{AE2} . This assumption will be tested and validated in Chapter 3.

In addition, the loss coefficient C_L also had to be updated to match with the assumptions stated above. In equation 2.25, C_L value refers to the loss coefficient through a single opening. But in the current model, the losses due to flow through openings are lumped for a specific area and hence, instead of loss coefficient for each opening, a single effective loss coefficient, K_L will be used (Guha, 2011). K_L can be estimated using the Bernoulli's obstruction theory (White, 1999) with a reasonable assumption that the area of the openings are much smaller, when compared to the total area of the panel array.

$$K_L = \frac{1 - (A_o/A)^2}{C_d^2} \quad (2.9)$$

Where A_o refers to the area of openings considered in the specific region, A refers to the total area of the specific region and C_d is the discharge coefficient through the lumped openings. The value of the discharge coefficient used in this study is 0.38 (Guha, 2011).

After considering all of the above mentioned changes above to the original discharge equations, the current model, which will be evaluated in this work, is:

$$\rho l_{e1} \dot{U}_{g1}(t) + K_{L1} \frac{\rho}{2} U_{g1}(t) |U_{g1}(t)| + \frac{12\mu l_{o1}}{G_1^2} U_{g1}(t) = P_{AE1}(t) - P_i(t) \quad (2.10)$$

$$\rho l_{e2} \dot{U}_{g2}(t) + K_{L2} \frac{\rho}{2} U_{g2}(t) |U_{g2}(t)| + \frac{12\mu l_{o2}}{G_2^2} U_{g2}(t) = P_{AE2}(t) - P_i(t) \quad (2.11)$$

$$A_1 U_{g1} + A_2 U_{g2} = 0 \quad (2.12)$$

where $U_{g1}(t)$ and $U_{g2}(t)$ refers to the velocities of flow in to and out of the cavity through the openings in regions 1 and 2, K_{L1} and K_{L2} represent the effective loss coefficients for regions 1 and 2, $P_{AE1}(t)$ and $P_{AE2}(t)$ are the area-averaged external pressures for the regions 1 and 2, respectively. $P_i(t)$ represents the uniform cavity pressure as mentioned in the assumptions in section 2.2.3.

Now consider the case in which the flow direction is not perpendicular to the face and the wind is coming towards the roof at an angle as shown in Figure 2.7. When the wind is coming at such an angle to the roof, the flow is separated at the edge in such a way that corner vortices form, as shown in Figure 2.7.

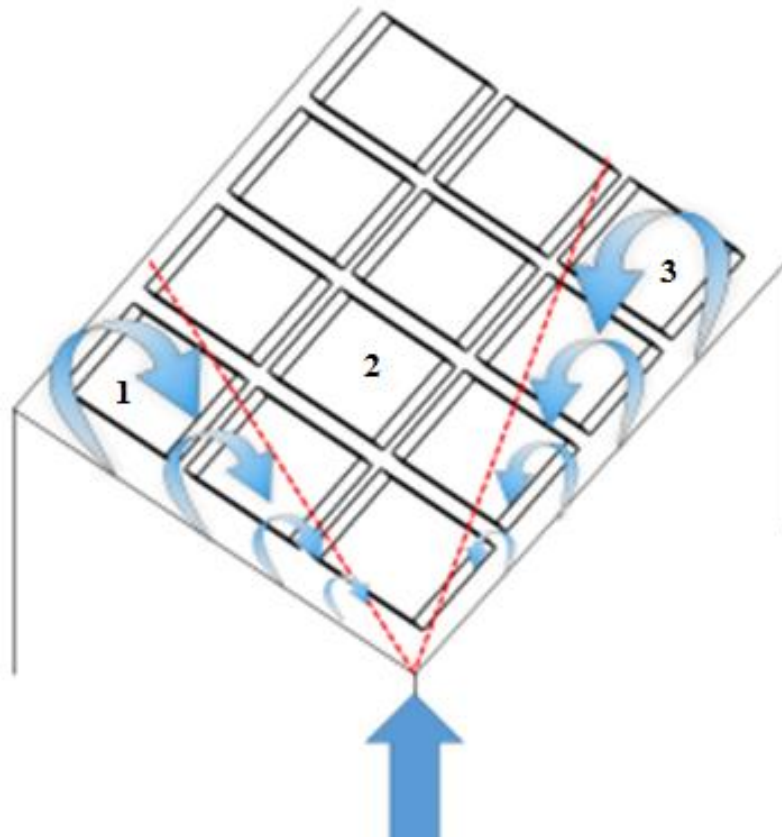


Figure 2-7: Schematic representation of flow separation and cavity flow when the wind direction is coming at an inclined angle to the roof

Due to the formation of corner vortices, the distribution of external pressures over the upper surface of the solar panels are different from the pattern discussed in the previous section. Since the wind is coming at an angle to the roof, corner vortices are generated along the two edges as shown in Figure 2-7. The corner vortices causes high sectional pressures along the edges and a relatively lower suction zone in the central portion of the roof. In this case it makes sense to think about three distinct pressure regions on the roof, which are labelled in Figure 2.7.

The estimation of cavity pressure in this scenario can be done using the following four equations

$$\rho l_{e1} \dot{U}_{g1}(t) + K_{L1} \frac{\rho}{2} U_{g1}(t) |U_{g1}(t)| + \frac{12\mu l_{o1}}{G_1^2} U_{g1}(t) = P_{AE1}(t) - P_i(t) \quad (2.13)$$

$$\rho l_{e2} \dot{U}_{g2}(t) + K_{L2} \frac{\rho}{2} U_{g2}(t) |U_{g2}(t)| + \frac{12\mu l_{o2}}{G_2^2} U_{g2}(t) = P_{AE2}(t) - P_i(t) \quad (2.14)$$

$$\rho l_{e3} \dot{U}_{g3}(t) + K_{L3} \frac{\rho}{2} U_{g3}(t) |U_{g3}(t)| + \frac{12\mu l_{o3}}{G_3^2} U_{g3}(t) = P_{AE3}(t) - P_i(t) \quad (2.15)$$

$$A_1 U_{g1} + A_2 U_{g2} + A_3 U_{g3} = 0 \quad (2.16)$$

In Chapter 3, this modeling approach will be tested and validated.

2.3 Details of the numerical simulation

For estimating the (uniform) cavity pressure, the unsteady discharge equations along with conservation of mass equation must be solved as described above. This requires a numerical method. In this study, a second-order, backward-differencing, numerical scheme is used (Chapra and Canale, 2006) where, at each time step, the given time series of the external pressures are used to solve for the (unknown) velocities through the gaps and the cavity pressure. The details of the numerical method, along with the algorithm for solving the equations, are explained in Appendix B.

The time varying pressure coefficients on the external or outer surface of the double layer system, $C_{pe}(t)$ are given by

$$C_{pe}(t) = \frac{P_e(t) - P_o}{\frac{1}{2} \rho \bar{V}_h^2} \quad (2.17)$$

where $P_e(t)$ is the external pressure time series obtained from the wind tunnel test, P_o is the static pressure and \bar{V}_h is the mean velocity at roof height. Similarly, the time varying pressure coefficient in the cavity is given by

$$C_{pi}(t) = \frac{P_i(t) - P_o}{\frac{1}{2} \rho V_h^2} \quad (2.18)$$

where $P_i(t)$ is the cavity pressure time series.

The area-averaged pressure coefficients are calculated by integrating the pressures of all taps within a specific area simultaneously. The area-averaged pressure coefficient for a given area for the external or upper surface is given by

$$C_{p_{AE}}(t) = \frac{\sum_{i=1}^n C_{p_E}(t) \cdot a_i}{A} \quad (2.19)$$

where $C_{p_E}(t)$ are the time history of the pressure coefficients on the upper or external surface of the module, a_i is the tributary area associated with the specific pressure tap 'i' and A is the sum of all tributary areas on one surface of the module.

The results obtained from the analytical model are validated by comparing the simulation results with the cavity pressures from the experimental study conducted on a roof-mounted solar panel array by Stenabaugh (2015), as discussed in Chapter 3.

Chapter 3

3 Results and Discussion

3.1 Introduction

In this chapter, the results from the analytical model are compared with the experimental results obtained from Stenabaugh (2015). The assumptions considered while developing the analytical model are also assessed.

3.2 Experimental set-up

The wind tunnel experiments for the solar panel array system were conducted in the Boundary Layer Wind Tunnel II at the University of Western Ontario by Stenabaugh (2015). Figure 3.1 shows the photo of a sloped roof model; however the results from the analytical model are compared with the experimental results obtained from a flat roof model as shown in Figure 3.4



Figure 3-1: Photo of the Boundary Layer Wind Tunnel at the University of Western Ontario along with the study model having solar panels on the sloped roof (Stenabaugh, 2015).

The wind tunnel has a working cross-section of 3.4m (11ft) wide by 2.4m (8ft) high along with an upstream fetch length of 39m (128ft). In the wind tunnel, an open country profile was simulated. The wind tunnel tests were conducted using 1/20 scale physical model. This scale was used because of the challenges in manufacturability of the panels and other practical issues associated with the solar panel module pressure tubing and spacing. The Reynold's number using the mean building roof height was about 3×10^5 and the blockage ratio of the physical model in the wind tunnel was 4.2%.

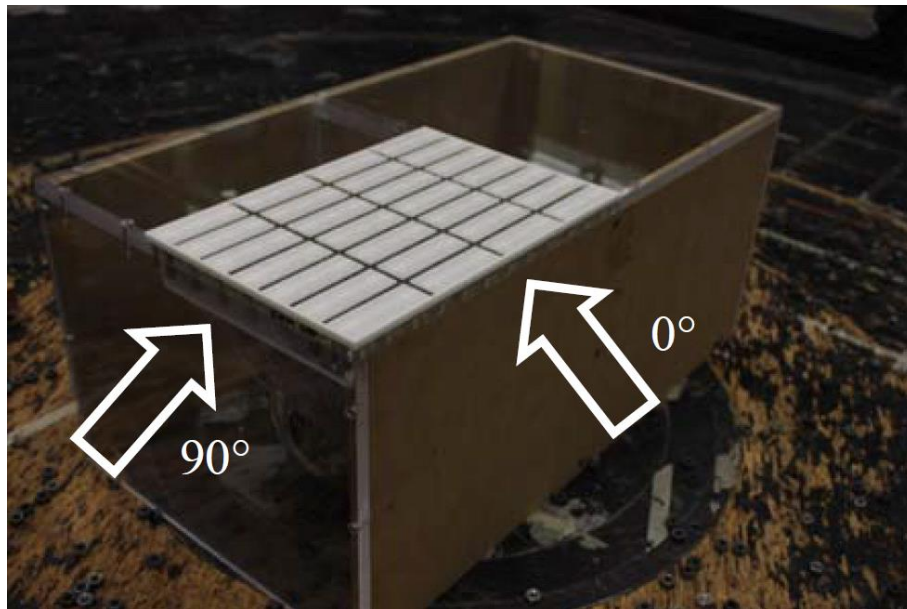


Figure 3-2: Wind tunnel physical model of the solar panel arrays on the flat roof surrounded by shroud (Stenabaugh (2015))

The solar panel modules were modeled as flat panels, made from white Delrin (acetyl) plastic, with equivalent full-scale dimensions of 50cm x 145.5cm, which gives an equivalent module area of 0.73 m^2 , as shown in Figure 3.3. The solar panel modules have a thickness of 0.3cm at a model scale of 1:20 and this was maintained to achieve the minimum thickness for the pressure tubes within them.

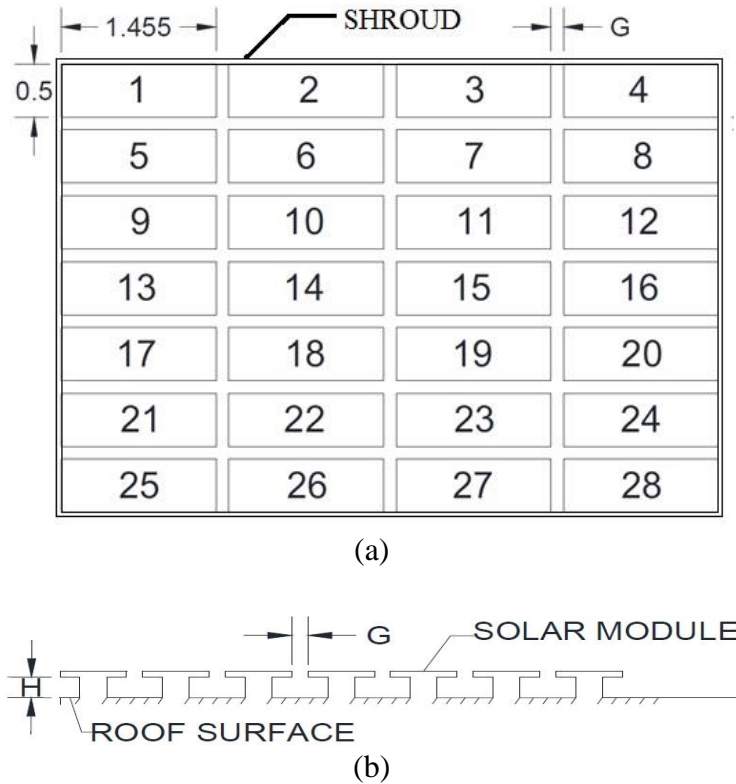


Figure 3-3: Drawings of the solar panel array showing the panel dimensions: (a) top view and (b) sectional view (Stenabaugh, 2015).

To obtain detailed information about the pressures acting on the external and internal surface of the solar panel array system, a high density pressure tap layout was required. With that intention, 20 pressure taps were placed on each individual solar panel module, i.e., 10 on the upper surface and 10 on the lower surface of each solar panel module by Stenabaugh (2015). Figure 3.4(a) shows the panel array of 28 modules used in the wind tunnel test and 3.4(b) shows a close-up view of a single panel (module) along with locations of pressure taps.

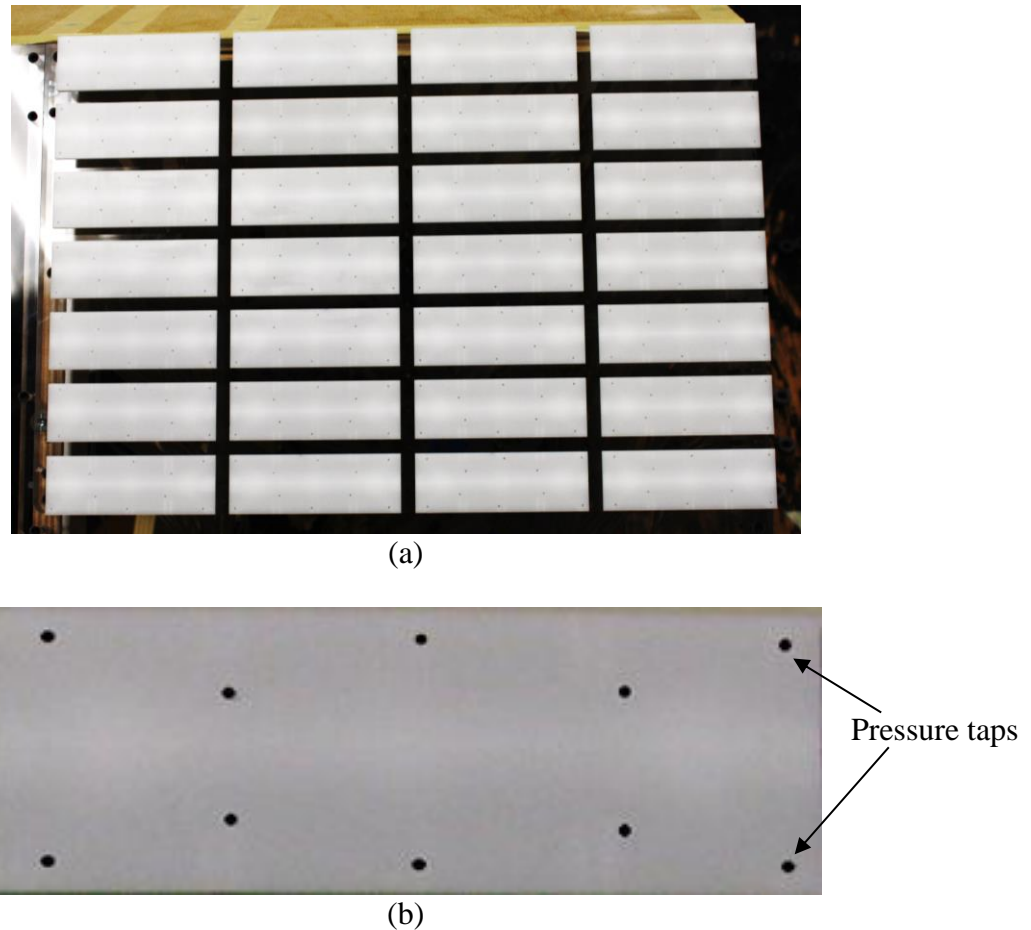


Figure 3-4: (a) Photos of the solar panel array system and (b) a close-up view of a single panel showing the position of pressure taps on the top surface of the panel (Stenabaugh, 2015).

During the wind tunnel test, experiments were carried out for different configurations and for different roofs. In the current study, we are comparing the results from the analytical model with the experimental results from flat roof configuration having a gap between the panels (G) equivalent to 12cm and the distance between the panel and the roof of 20cm.

The flat roof model used in the wind tunnel test has full-scale dimensions of 15m x 7.5m along with an eave height of 6m. The solar panel array was located at the corner of the flat roof, adjacent to the walls so that it would experience maximum suction due to the flow separations. As mentioned in section 2.2.3, the results from the analytical model have to be compared with experimental data in which the flow into or out of the cavity can

happen only through the gaps between the panel modules. For that purpose, the experimental configuration in which the solar array was surrounded by a shroud, as shown in Figure 3.2, was selected. The bottom of the shroud was sealed to the roof surface and the top of the shroud was flush with the top level of solar panels.

During the wind tunnel tests, the pressure measurements were made at a reference speed of approximately 14 m/s, which corresponds to a mean wind speed at the mean roof height of 42 m/s in full scale, based on a velocity scale of 1:3. The wind tunnel measurements were collected for 16 wind directions in 22.5° increments. The pressure data samples were collected for 360 seconds at a sampling rate of 400 samples per second, which is equivalent to a full-scale sampling period of approximately 40 minutes. A low-pass filter was used to filter the data at 200 Hz.

3.3 Assumptions considered in the analytical model

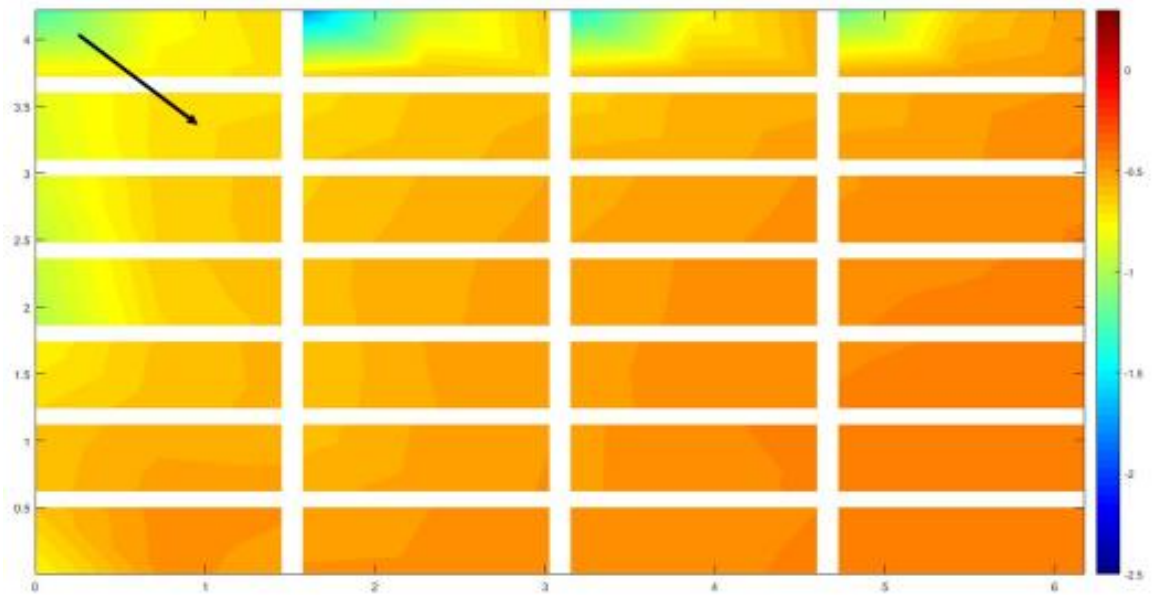
Before presenting the comparison of predicted results with the experimental data, it is important to ensure that the assumptions considered during the development of the analytical model are correct. The primary assumption of uniform cavity pressure in double layer systems is the most important one.

3.3.1 Validation of the assumptions considered in the analytical model

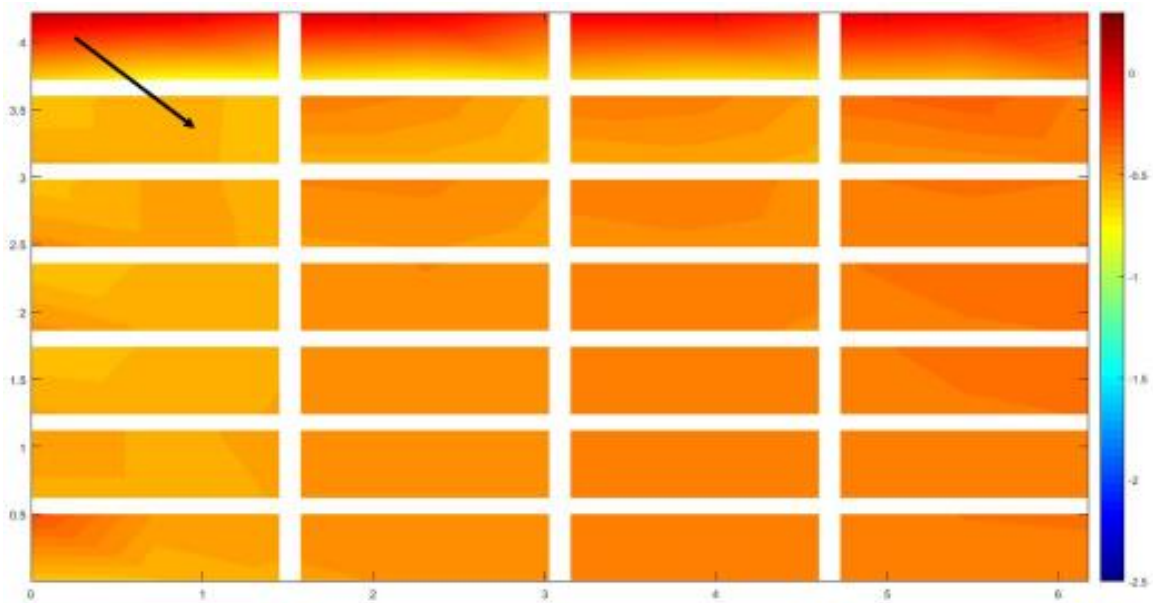
The mean pressure distribution for external and cavity pressures obtained from the wind tunnel test results for a few angles are compared. The contour plots for the wind direction of 135 degrees are shown in Figure 3.5. From the contour plots in Figure 3.5 (a), it is clear that, at the building edge, the flow is separated and the external surface of the solar panels are subjected to higher suction due to the formation of corner vortices, as shown in Figure 2.6.

However, the mean distribution of cavity pressure values obtained from wind tunnel test, shown in Figure 3.5 (b) have a more uniform distribution throughout the panel array, except at a few locations. There are a few locations in the cavity that show slight variation to the uniform pressure assumption and it may be due to some localized flows through the gaps.

But generally, looking at the overall pressure distribution, it is reasonable to consider a uniform pressure distribution in the cavity. Any deviations from uniformity will lead to inaccuracies in the modeling approach, and consequent errors in the modeling of the net wind loads on the outer layer.



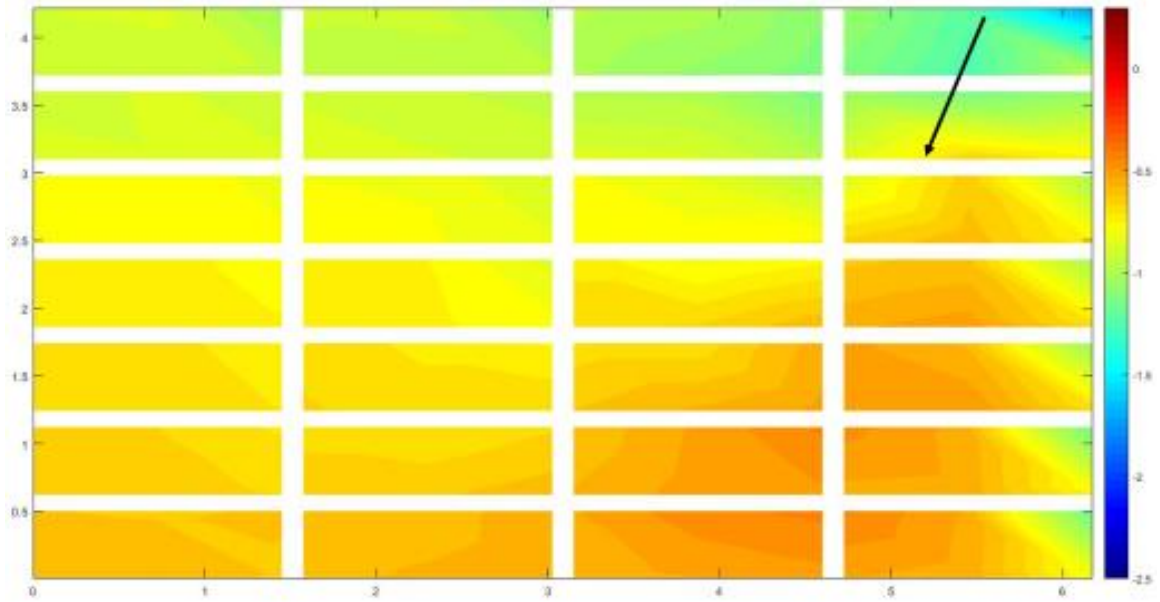
(a)



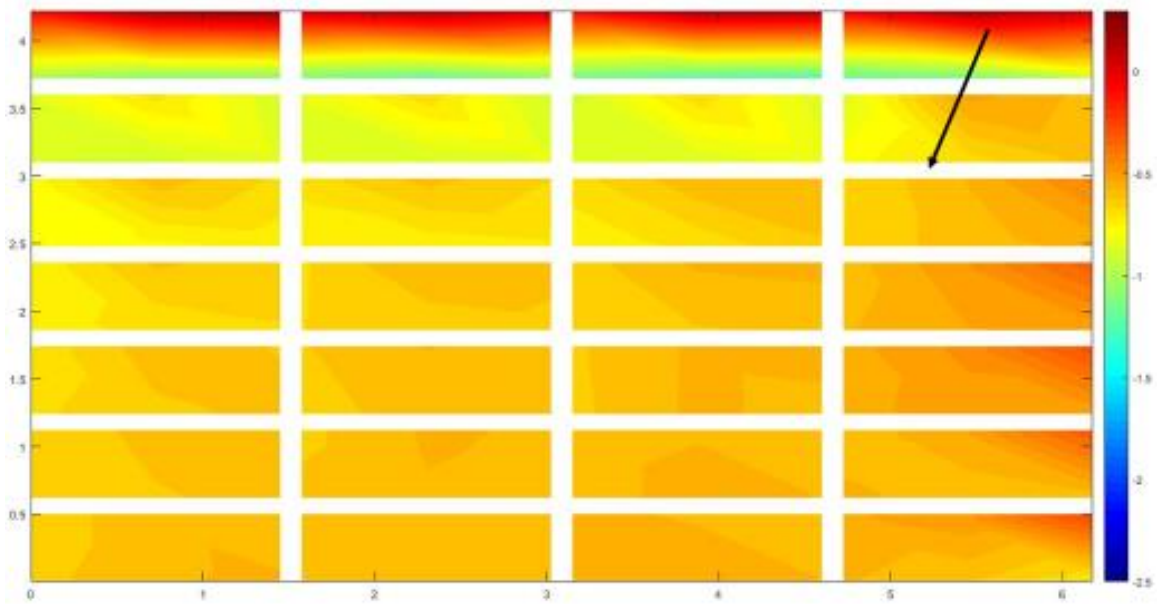
(b)

Figure 3-5: The mean pressure distribution for 135 degree wind direction for (a) external and (b) cavity pressures.

Similarly the external pressure distribution values are compared with the cavity pressure distribution for some other wind directions, 203, 225 and 315 degrees. The contour plots comparing the pressure distributions of external and cavity surfaces are shown in Figures 3.6, 3.7 and 3.8. As explained earlier, for 135 degrees, the external pressure distributions for most of the wind directions have the similar pattern, i.e., the cavity pressure values can be considered as being close to uniform for most of the locations and for the majority of the angles. There are a few exceptions, as mentioned in previous section.

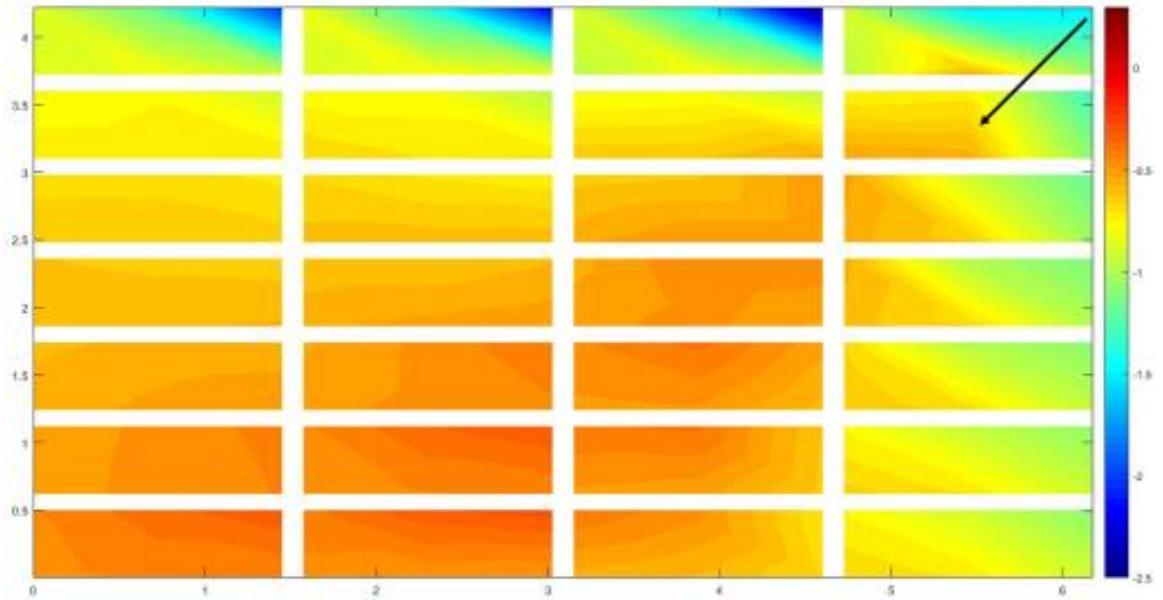


(a)

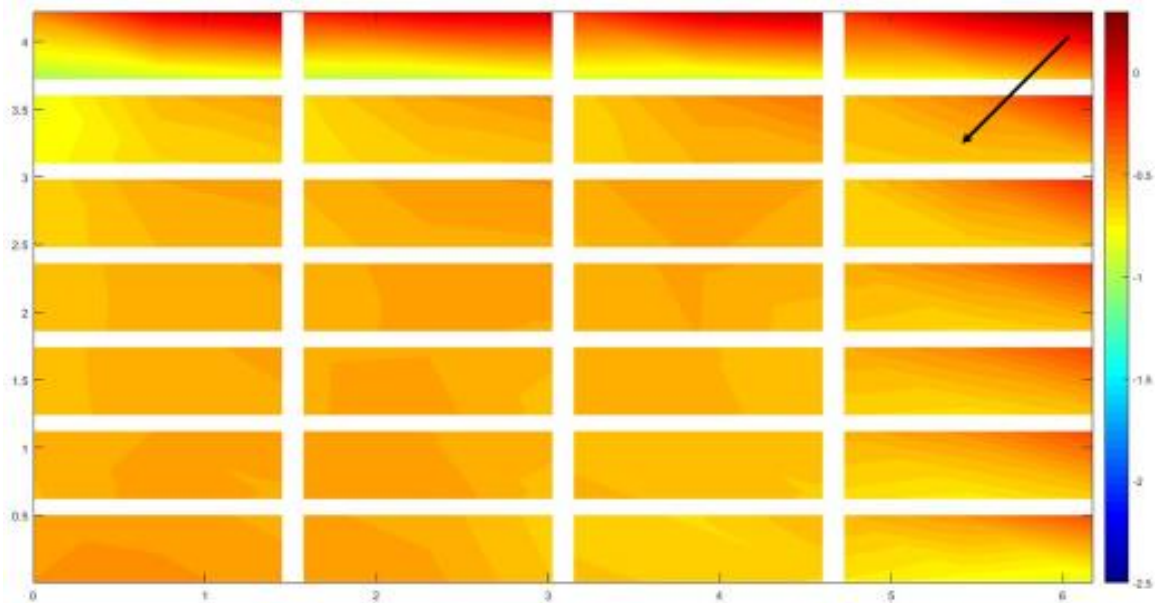


(b)

Figure 3-6: The mean pressure distribution for 203 degree wind direction for (a) external and (b) cavity pressures.

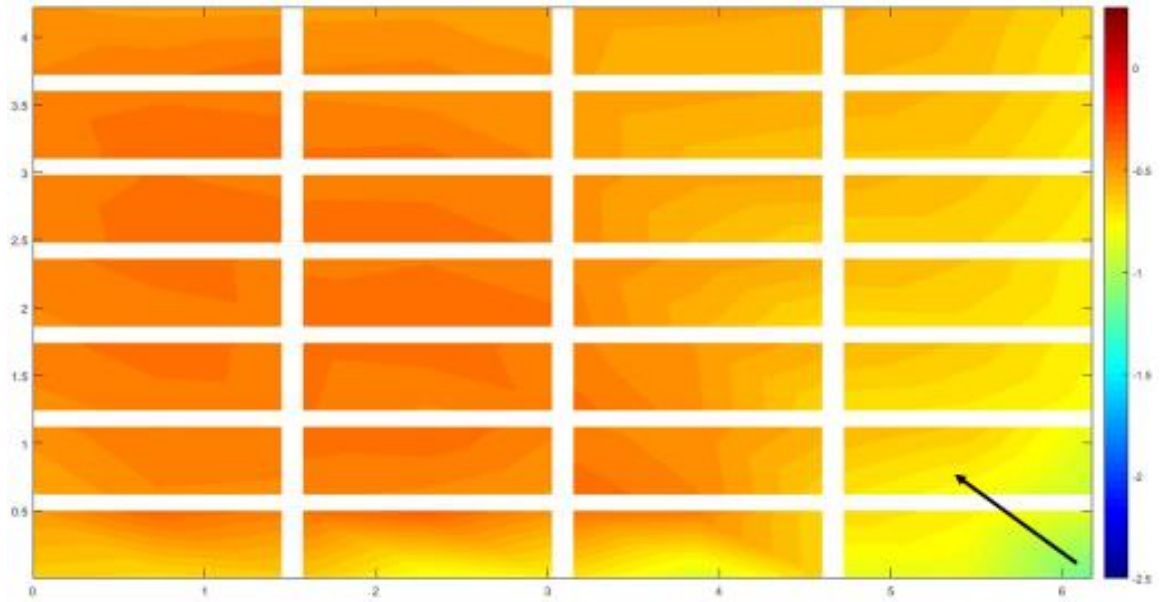


(a)

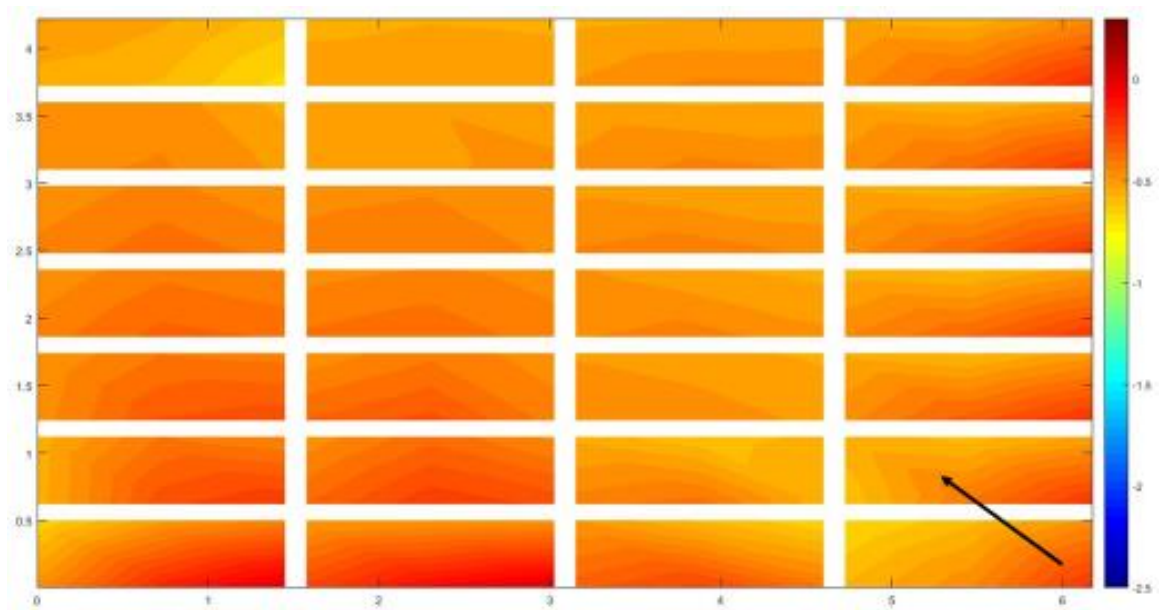


(b)

Figure 3-7: The mean pressure distribution for 225 degree wind direction for (a) external and (b) cavity pressures.



(a)



(b)

Figure 3-8: The mean pressure distribution for 315 degree wind direction for (a) external and (b) cavity pressures.

3.4 Method

As mentioned in Section 2.2, the analytical model uses orifice discharge equation and conservation of mass equation for estimating the cavity pressure in double-layered systems. The step-by-step procedure of the working of analytical model are shown in the form of a flowchart in Figure 3-9. The first step is to examine the pressure distribution on the external surface of the panel array, which is obtained from the wind tunnel tests. The mean external pressure distribution is a crucial factor which decides the average flow through the openings and the location of neutral pressure line. The second step is estimating location of the neutral pressure line. Initially, since the cavity pressure is unknown, the spatial average of all the external pressures is taken as the cavity pressure. This allows one to set a neutral pressure line and based on its location, the areas of flow entry and exit are decided. In reality, these areas can be quite complicated and, hence, the areas are simplified into rectangular or triangular shapes, depending upon the wind direction and pressure distribution pattern. Then, the governing equations, mentioned in the previous section, are solved for each of the simplified areas, using the numerical method. Once the equations are solved, one obtains the cavity pressure. At that point, one needs to check whether the flow directions and regions are more precise with the actual distribution. If the predicted cavity pressure are sufficiently accurate, then we can proceed with the calculation of net wind loads. If the predicted cavity pressure is too different than the actual pressure, then the model must be recalculated from the second step, i.e., setting the neutral pressure line. The user then uses the model results to decide the neutral pressure line based on the cavity pressure obtained from the first iteration and this whole process is continued until a sufficiently accurate cavity pressure is obtained.

The flowchart in Figure 3-9 shows the framework for the analytical model. In this study, the results from the lumped leakage approach were compared with the experimental results. But in the case of using this method as a practical tool, more detailed investigations are needed, especially on how to make sure that the neutral pressure line matches with real condition. Also, the iteration process, which changes the location of neutral pressure line, needs to be investigated in detail.

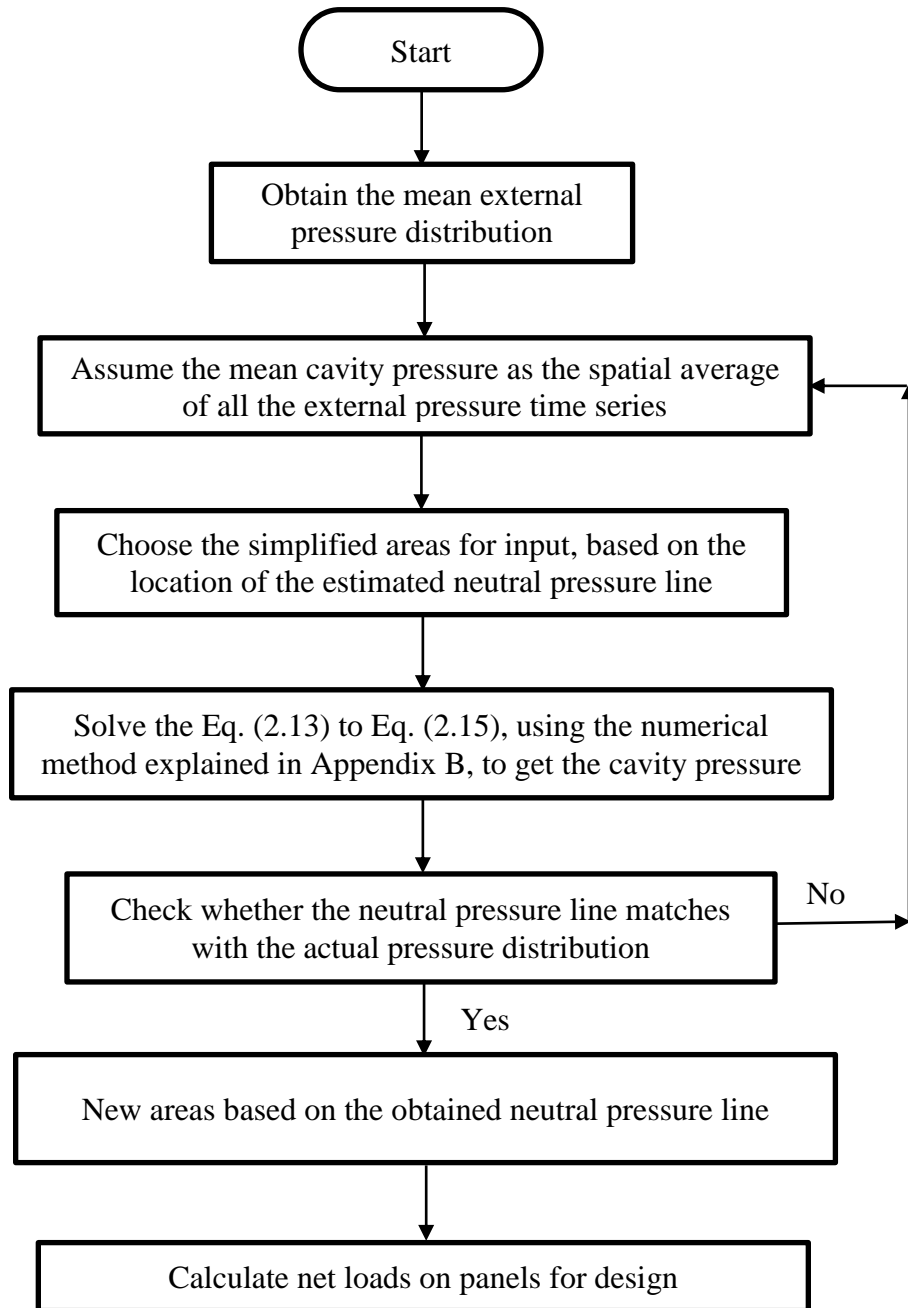


Figure 3-9: Flow chart showing the algorithm of the analytical model

3.4.1 Consideration of simplified areas as input for the model

As mentioned in the flow chart in Figure 3-9, the area-averaged external pressures are calculated for simplified areas based on the location of the neutral pressure line and simplified areas, for four wind directions, are shown in Figure 3-10. In this study, the simplified areas are triangular. This is because for all four wind directions, which are coming at an angle to the roof, the three areas for area-averaging are chosen in such a way that two will be representing the corner vortices whereas the third one should be representing the central zone between the corner vortices. As shown in Figure 3-10, the corner vortices have significant gradients, whereas the central pressure zone is almost uniform, which is natural for pressure distributions on roofs. The neutral pressure lines considered in this study are shown as dotted lines in Figure 3-10 and the area in each of those specified regions were considered for the estimation of area-averaged external pressure. Since this was the first attempt to check whether the lumped-leakage approach can be used to estimate the cavity pressure, the neutral pressure lines were chosen manually.

In the current study, the selection of simplified areas was done manually, by considering the pattern of external pressure distribution and angle of wind direction. This was done manually to check whether the concept mentioned in Figure 3-9 could work. The automation of this step would be the next step and that process will depend on many constraints based on the application. For example, the process for solar panel array on roof will be different from a high-rise cladding system. But those points will be considered as a future recommendation and currently we are focusing on the validation of the concept.

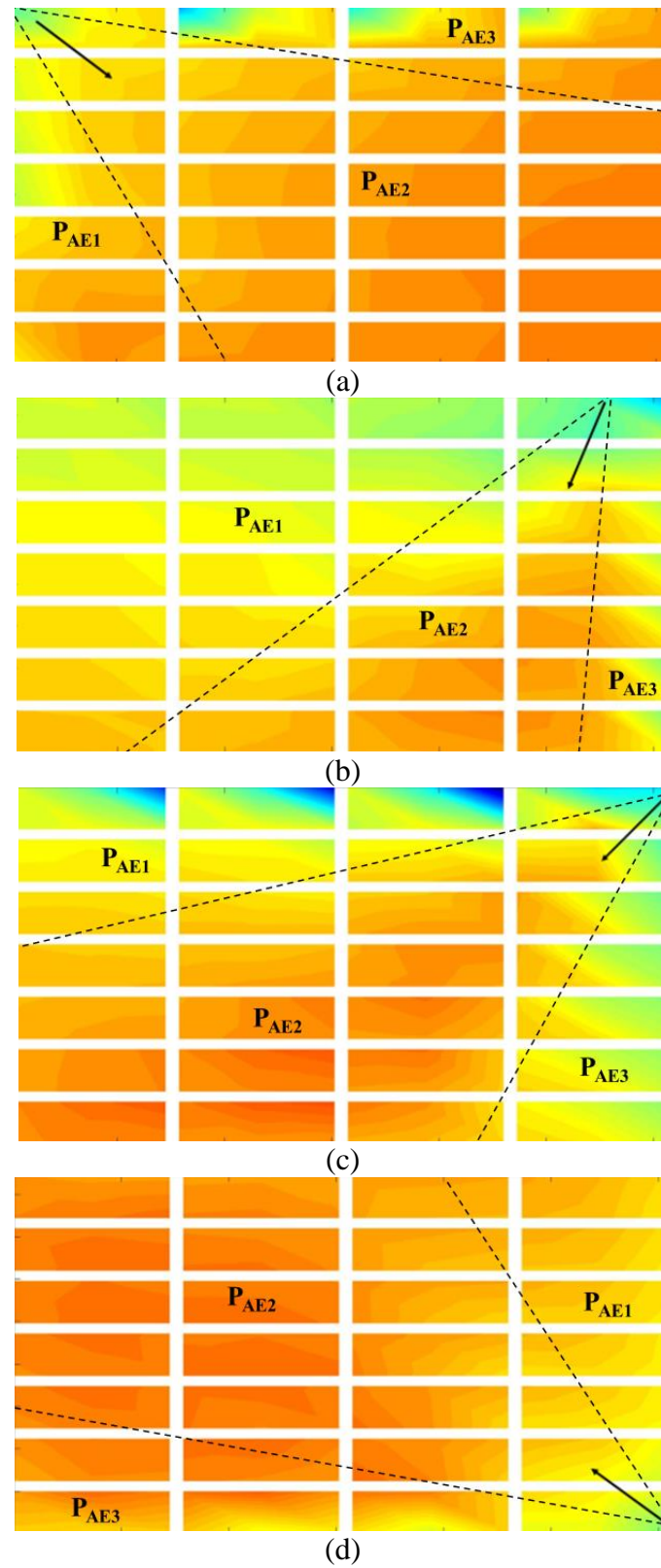


Figure 3-10: Areas considered for the area-averaged external pressures for various wind directions (a) 135 degree (b) 203 degree (c) 225 degree and (d) 315 degree

3.5 Results

3.5.1 Comparison of time-series and spectra of area-averaged pressure coefficients

The cavity pressure time histories are estimated by applying the lumped-leakage approach to the orifice flow equations as explained in Chapter 2. A segment of the time history is shown for a wind direction of 135 degrees in Figure 3.11. The time history for the experiments is obtained via an area-average of the measured cavity pressures. There is good agreement between the predicted values and the experimental results and the results showed that the analytical model can capture the variations and distribution of cavity pressure, although there are clearly some differences. Figure 3.12 shows the comparison of the spectra from the numerical model and the experimental results, which match well over the range of relevant frequencies.

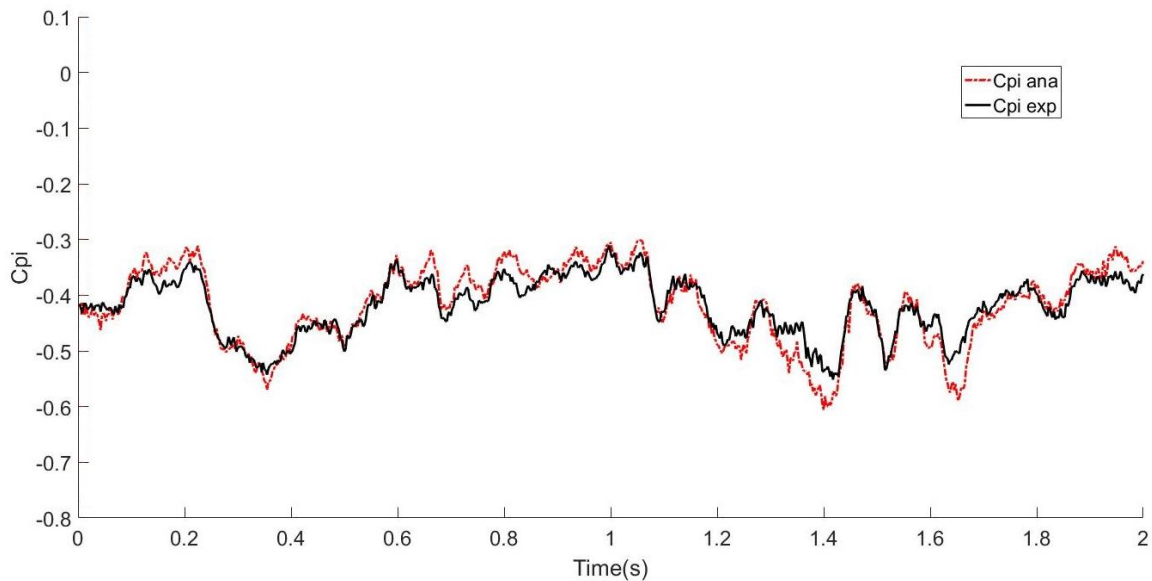


Figure 3-11: Comparison of time series obtained from analytical model with the experimental results for a wind direction of 135 degrees.

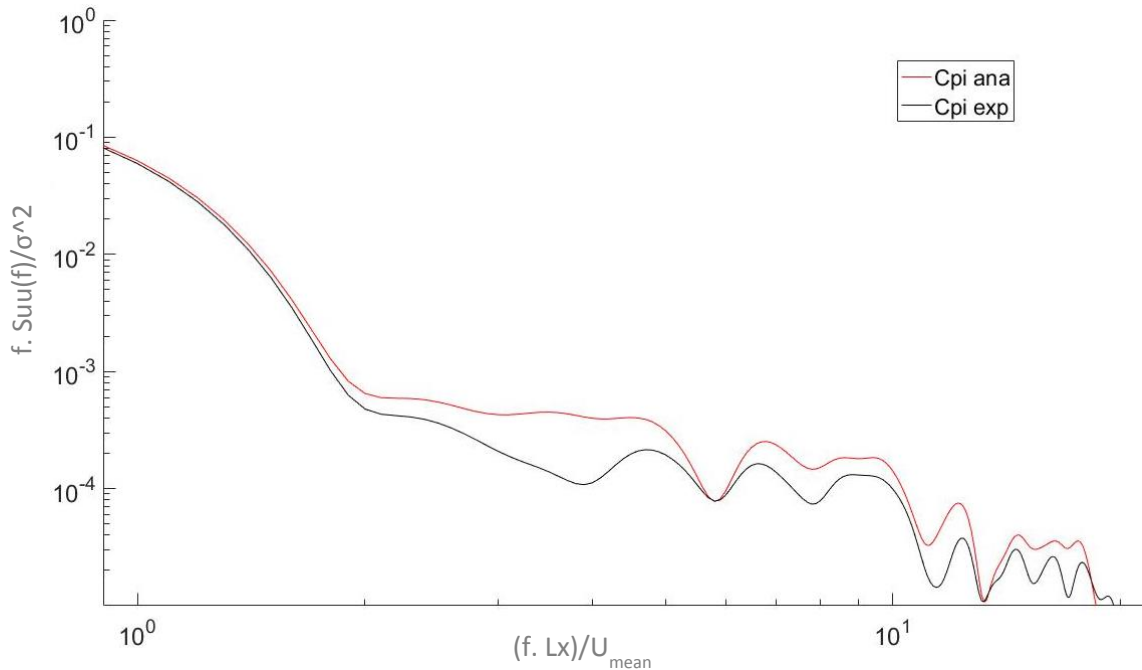


Figure 3-12: Spectra comparison of analytical results with the experimental results for 135 degree wind direction

Table 3-1 shows the statistical comparison of the predicted values with the experimental results. From the values in the table, it is clear that there is good agreement between the predicted and experimental results. The similarity between the experimental values and predicted values are not only in mean values. Standard deviation, maximum and minimum values from both time series are compared and the results showed that the predicted cavity pressure time series are similar to the experimental values, with the analytical results within about 5% of the experimental. The model results tend to underestimate the experimental for the overall fluctuations, but since the model tends to over-estimate at the higher frequencies, the peak values are also over-estimated in magnitude.

Table 3-1: Statistical comparison of results obtained from the analytical model with the spatially averaged time-series obtained from the wind tunnel test.

Wind Direction	Pressure	Mean	RMS	Max	Min
135°	$Cp_{AE}(t)$	-0.561	0.088	-0.256	-1.084
	Cp_i from wind tunnel test	-0.447	0.061	-0.225	-0.806
	Cp_i from analytical model	-0.434	0.059	-0.208	-0.843
	Ratio of Analytical result to wind tunnel result	0.97	0.96	0.92	1.05
203°	$Cp_{AE}(t)$	-0.754	0.114	-0.399	-1.271
	Cp_i from wind tunnel test	-0.610	0.088	-0.287	-1.015
	Cp_i from analytical model	-0.582	0.085	-0.301	-1.071
	Ratio of Analytical result to wind tunnel result	0.95	0.97	1.05	1.06
225°	$Cp_{AE}(t)$	-0.689	0.100	-0.318	-1.212
	Cp_i from wind tunnel test	-0.538	0.074	-0.226	-0.910
	Cp_i from analytical model _i	-0.518	0.068	-0.244	-0.919
	Ratio of Analytical result to wind tunnel result	0.96	0.92	1.08	1.01
315°	$Cp_{AE}(t)$	-0.524	0.064	-0.308	-0.833
	Cp_i from wind tunnel test	-0.444	0.053	-0.244	-0.714
	Cp_i from analytical model _i	-0.418	0.049	-0.235	-0.747
	Ratio of Analytical result to wind tunnel result	0.94	0.93	0.97	1.05

Similarly, the time series from the predicted results and the experimental results are compared for a few more wind angles and the results are shown in Figure 3.13 through Figure 3.18. For the 135-degree wind direction results, there is, again, good agreement between the predicted time series obtained from the analytical model and the experimental results. The comparison of mean, standard deviation, maximum and minimum of the experimental and predicted values of external pressure and cavity pressures for all the four wind directions are shown in Table 3-1. From the comparison of results, it is clear that there is a good statistical agreement between the predicted and experimental values.

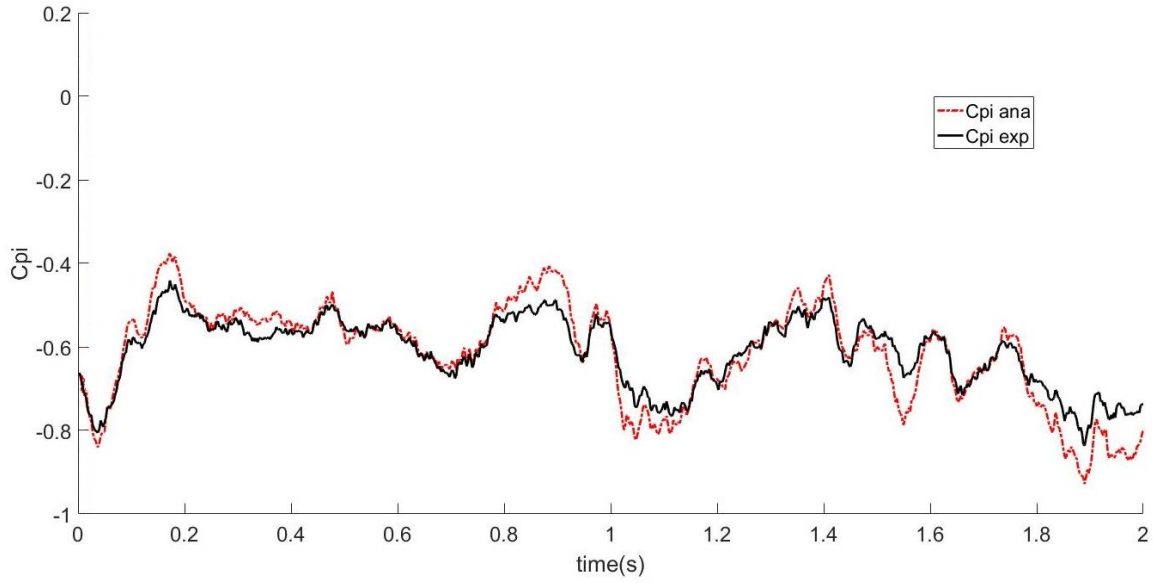


Figure 3-13: Comparison of time series obtained from analytical model with the experimental results for 203-degree wind direction.

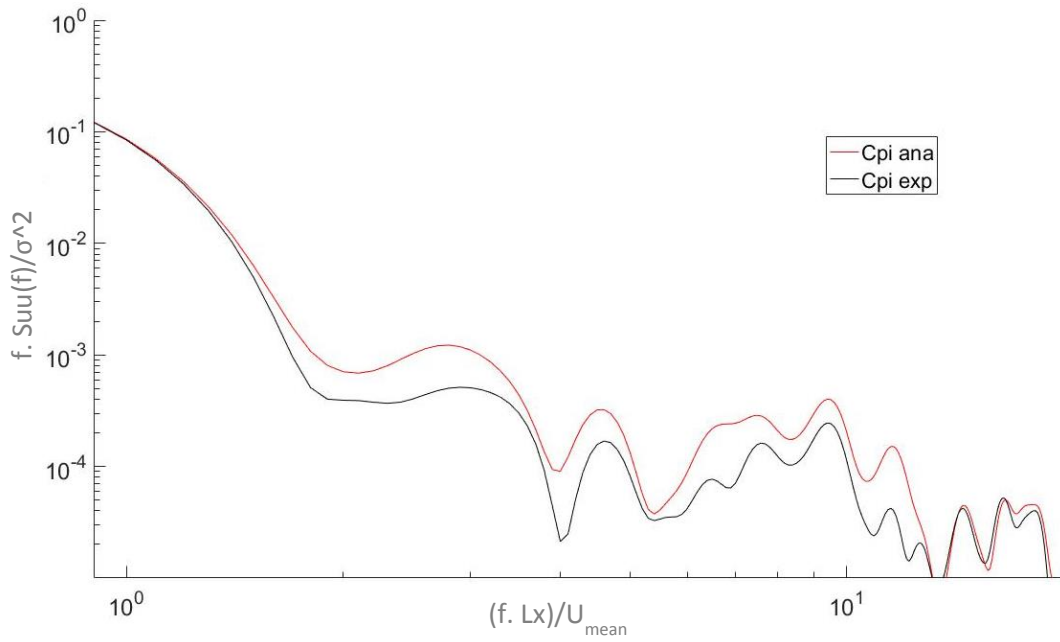


Figure 3-14: Spectra comparison of analytical results with the experimental results for 203-degree wind direction.

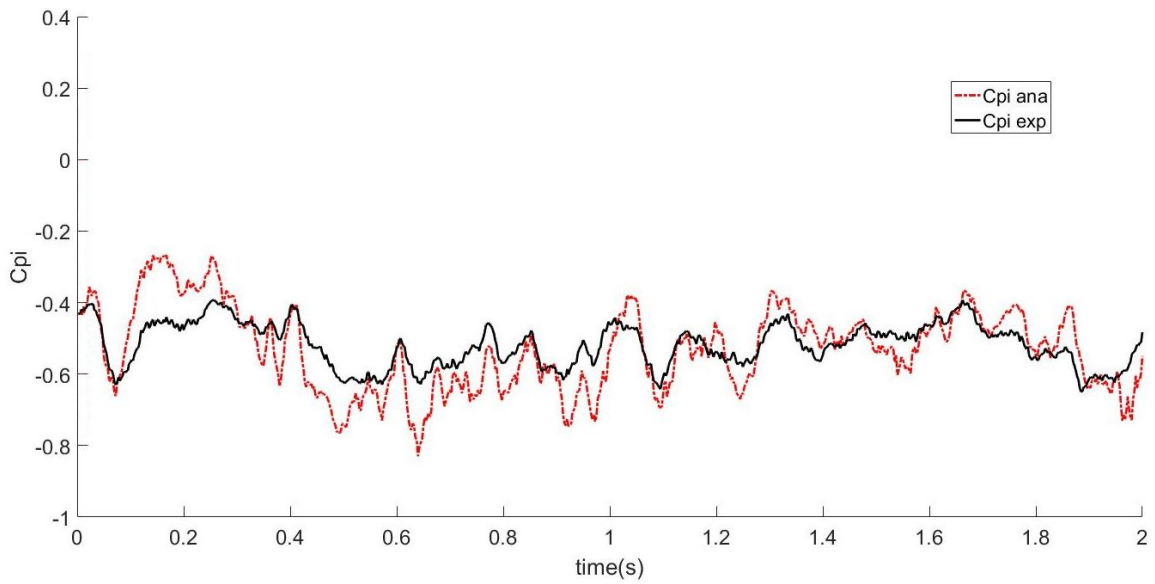


Figure 3-15: Comparison of time series obtained from analytical model with the experimental results for 225-degree wind direction.

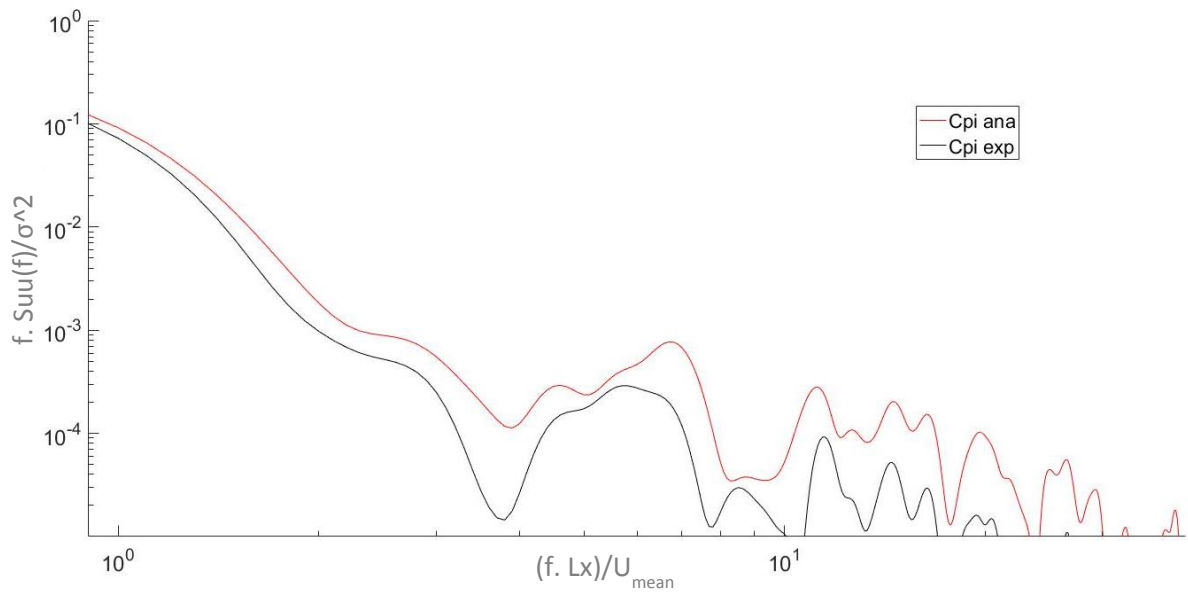


Figure 3-16: Spectra comparison of analytical results with the experimental results for 225-degree wind direction.

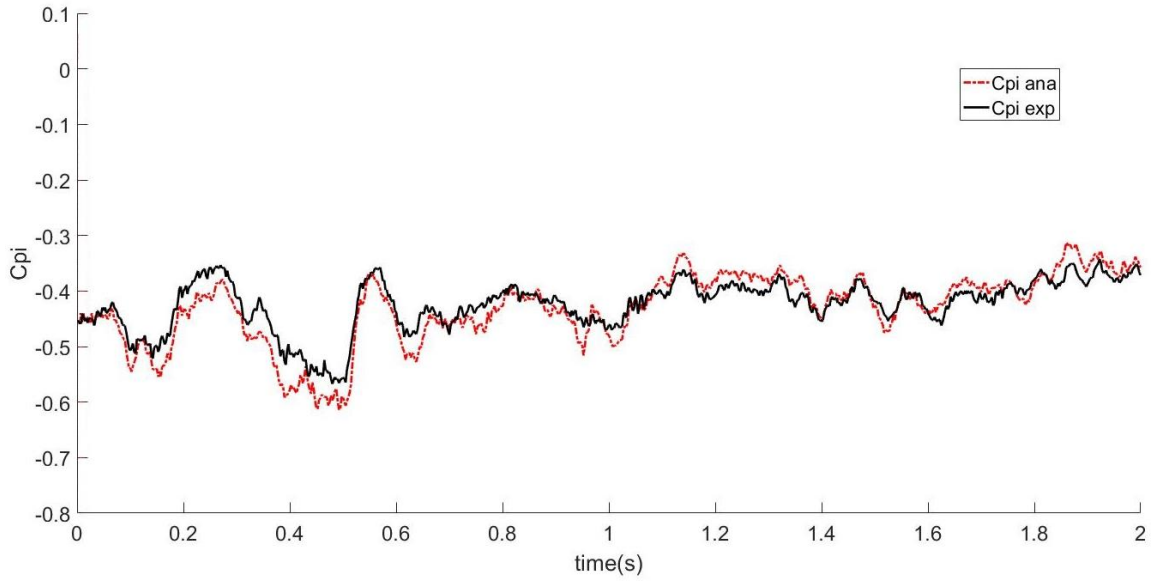


Figure 3-17: Comparison of time series obtained from analytical model with the experimental results for 315-degree wind direction.

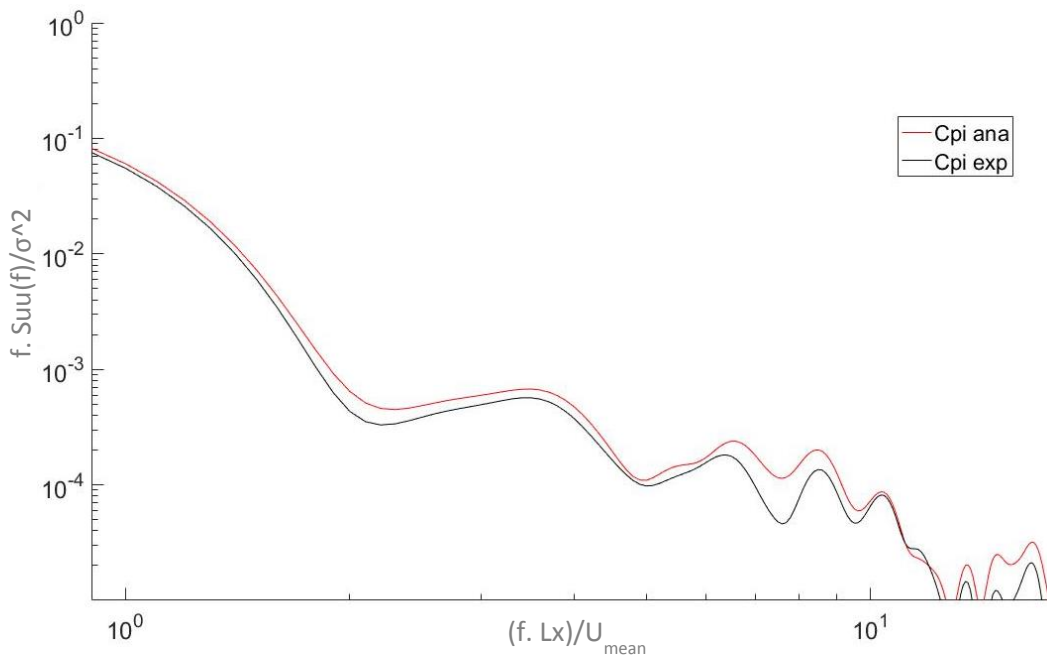


Figure 3-18: Spectra comparison of analytical results with the experimental results for 315-degree wind direction.

3.5.2 Comparison of predicted cavity pressure time-series with individual cavity pressure tap time series

In section 3.4.1, the time series obtained from the analytical model using the equations mentioned in chapter 2 are compared with cavity pressure time series. Both these time-series are area-averaged with respect to the whole array (or cavity) area. In this section, the area-averaged time series obtained from the analytical model are compared with the individual pressure taps in the cavity. Figure 3-19 shows the distribution of correlation coefficients between the external and cavity pressure tap time series, for 225 degree wind direction, and both these time series used for the calculation of correlation coefficients are taken from the wind tunnel experiment of Stenabaugh (2015). There are a few low values along the top edge of the panel arrays which may be due to the significant difference in pressure values, as shown in Figure 3-7.

0.68	0.01	-0.36	0.01	-0.13	-0.44	0.20	-0.25	-0.45	0.04	-0.38	-0.16
0.80	0.71	0.33	0.78	0.73	0.47	0.65	0.83	0.56	0.67	0.71	0.77
0.82	0.46	0.21	0.59	0.48	0.19	0.61	0.57	0.21	0.41	0.23	-0.07
0.82	0.82	0.76	0.82	0.78	0.79	0.81	0.82	0.65	0.83	0.88	0.79
0.79	0.64	0.43	0.73	0.64	0.57	0.78	0.40	0.38	0.65	0.52	-0.01
0.87	0.85	0.73	0.87	0.86	0.72	0.84	0.81	0.70	0.86	0.89	0.80
0.88	0.69	0.53	0.79	0.65	0.58	0.66	0.32	0.22	0.65	0.52	0.01
0.90	0.82	0.75	0.88	0.84	0.64	0.87	0.85	0.76	0.85	0.91	0.81
0.87	0.66	0.55	0.76	0.45	0.26	0.53	0.18	0.17	0.63	0.46	0.01
0.85	0.78	0.64	0.90	0.85	0.64	0.90	0.86	0.77	0.85	0.92	0.80
0.84	0.62	0.40	0.68	0.36	0.07	0.48	0.15	0.28	0.63	0.47	-0.04
0.84	0.83	0.66	0.91	0.85	0.70	0.90	0.84	0.81	0.86	0.90	0.79
0.91	0.91	0.91	0.91	0.91	0.91	0.91	0.91	0.91	0.91	0.91	0.91
0.91	0.91	0.91	0.91	0.91	0.91	0.91	0.91	0.91	0.91	0.91	0.91

Figure 3-19: Distribution of the external and cavity pressure correlation coefficients from the experimental results

In Figure 3-20, the distribution of correlation coefficients between the external pressure tap time series and the cavity pressure time series are plotted for 225 degree wind direction, in which the external time-series are the same as those in the Figure 3-19, whereas the cavity pressure time series are those obtained from the analytical model.

0.76	0.58	0.64	0.91	0.74	0.63	0.90	0.85	0.76	0.81	-0.41	-0.21
0.73	0.66	0.81	0.81	0.59	0.95	0.75	0.79	0.51	0.73	0.74	0.79
0.79	0.59	0.32	0.65	0.35	0.11	0.47	0.45	0.09	0.26	0.19	-0.05
0.65	0.59	0.65	0.74	0.69	0.69	0.68	0.75	0.47	0.69	0.71	0.65
0.63	0.59	0.37	0.36	0.52	0.43	0.70	0.36	0.29	0.53	0.50	-0.03
0.79	0.8	0.69	0.75	0.68	0.61	0.72	0.71	0.70	0.79	0.67	0.72
0.80	0.73	0.59	0.80	0.63	0.55	0.66	0.47	0.19	0.64	0.49	0.57
0.86	0.12	0.73	0.82	0.86	0.67	0.88	0.78	0.71	0.84	0.69	0.74
0.82	0.65	0.69	0.80	0.53	0.35	0.59	0.25	0.31	0.74	0.51	0.05
0.78	0.81	0.56	0.87	0.88	0.75	0.80	0.81	0.69	0.74	0.84	0.85
0.81	0.59	0.54	0.74	0.49	0.09	0.58	0.19	0.33	0.78	0.52	-0.09
0.84	0.78	0.59	0.87	0.69	0.81	0.85	0.79	0.74	0.69	0.87	0.71
0.72	0.72	0.73	0.70	0.71	0.71	0.70	0.72	0.72	0.72	0.72	0.72
0.71	0.71	0.73	0.71	0.76	0.69	0.71	0.73	0.72	0.74	0.73	0.74

Figure 3-20: Distribution of the external and cavity pressure correlation coefficients from the analytical model

From the comparison of correlation coefficients plotted in Figure 3-19 and 3-20, it is clear that there is a reasonable agreement between the correlation coefficients in most of the locations, especially in the regions of uniform cavity pressure. There are a few locations in the panel array where there are discrepancies in correlation coefficient values which indicates the disagreement between the actual cavity pressure time series and the predicted one. The discrepancies may be due to the approximations considered in the analytical model or also due to some of the pressure values which are entirely off from the rest of the values. Moreover, it has to be accounted that the cavity pressure time series used in Figure 3-19 was the individual cavity pressure tap time series whereas the one used for the calculation of correlation coefficient in Figure 3-20 was the area-averaged time series obtained from the analytical model.

3.5.3 Comparison of net pressure distributions

The most important parameter considered for the design of solar panel systems, especially in the case of wind loading, are the net loading across the panels as both the external (upper) surface and the cavity (lower) are exposed to wind. Net loading is the difference between the pressures on the upper and lower surfaces and it is what is required for the design of mounting and support systems for the solar panel arrays.

In Figure 3-21 (a), the mean net pressures are plotted for the 135-degree wind direction, i.e., the difference between the external pressures and the cavity pressures obtained from the wind tunnel experiment, whereas Figure 3-21 (b) shows the values obtained from the analytical model. The primary differences between the experimental and predicted values are near the top left corner of panels in the first row, which may be due to the non-uniformity of cavity pressures along that region. The cavity pressures in that region have some high values due to the localized flows through the gaps, as mentioned in section 3.4.1.

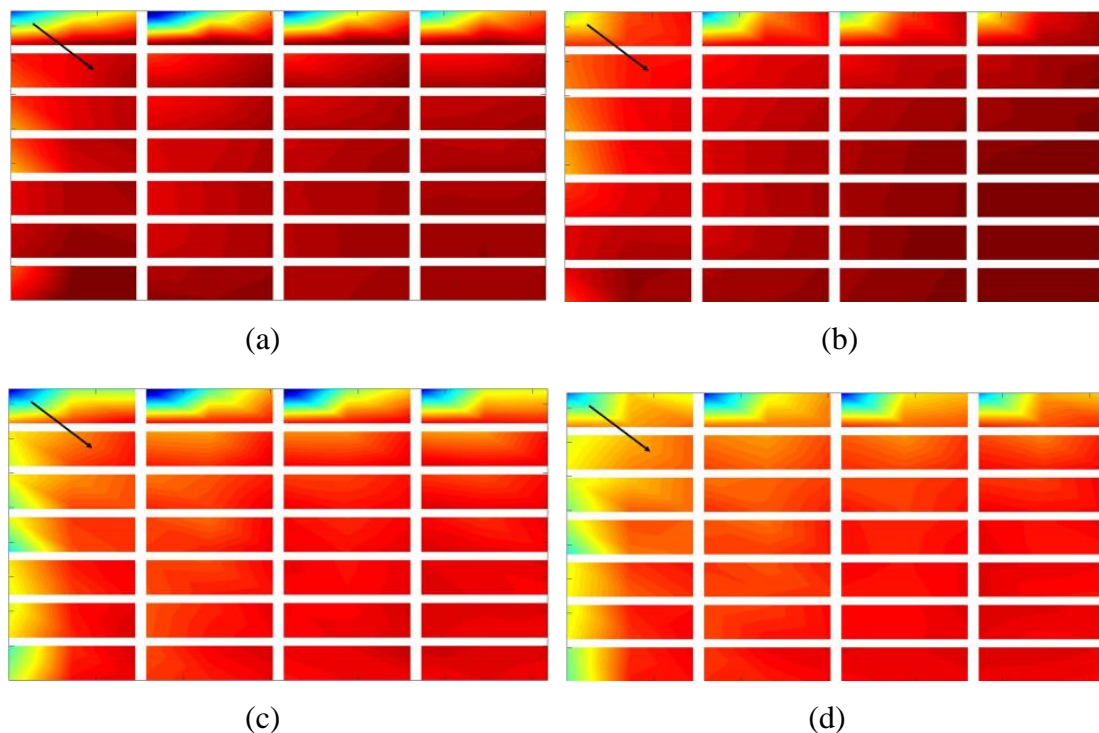


Figure 3-21: Contour map of net pressure distributions for the 135-degree wind direction for (a) experimental and (b) analytical mean net pressures and for (c) experimental and (d) analytical peak net pressures.

Figure 3-21 (c) shows the peak net loads, for the 135-degree wind direction, from the experimental and the predicted cavity pressures. The peak net pressure coefficients are statistically calculated using Lieblein BLUE method (Lieblein, 1974). In this method, the time-series will be divided into ten equal segments and picking the peak value from each of the ten segments. The mode and dispersion are calculated using the peak values and

Type I extreme value distribution can be used to estimate a more reliable peak for the entire time series.

The results show the same pattern as observed for the mean net pressure comparisons. There is a strong agreement between the experimental and predicted peak net pressures for most of the regions in the panel where the cavity pressures are uniform. Similar to mean net pressure distribution, there are some differences in peak net pressures along the top left edge values due to the high cavity pressures.

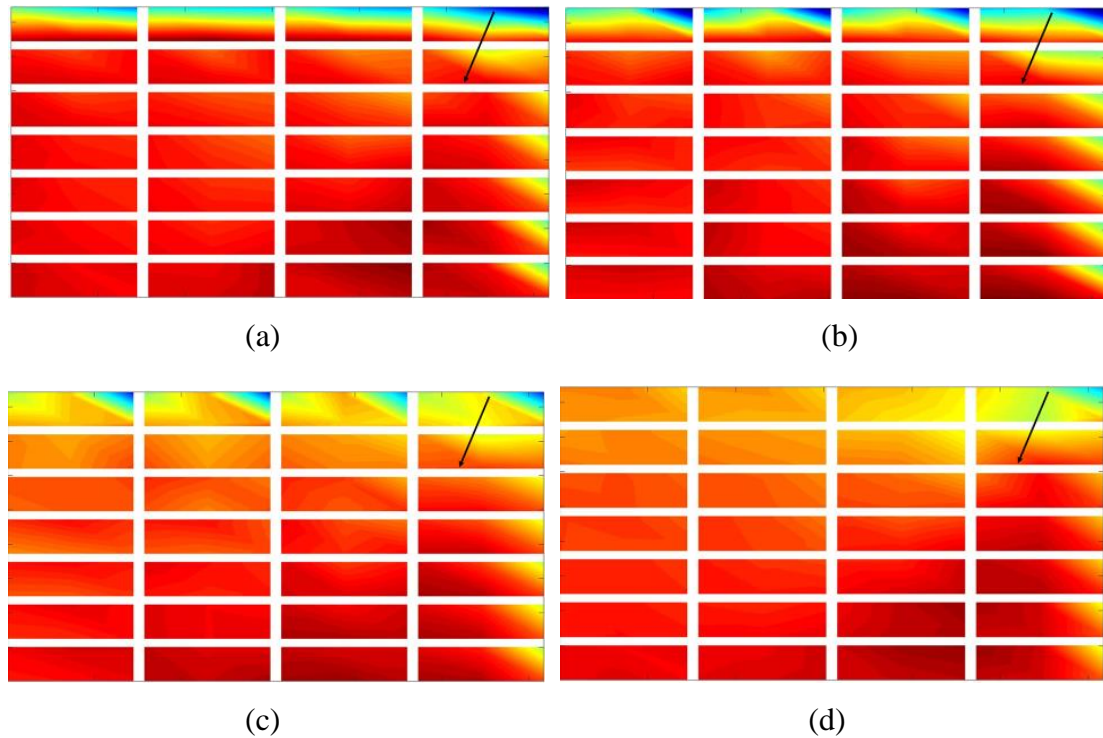


Figure 3-22: Contour map of net pressure distributions for the 203-degree wind direction for (a) experimental and (b) analytical mean net pressures and for (c) experimental and (d) analytical peak net pressures.

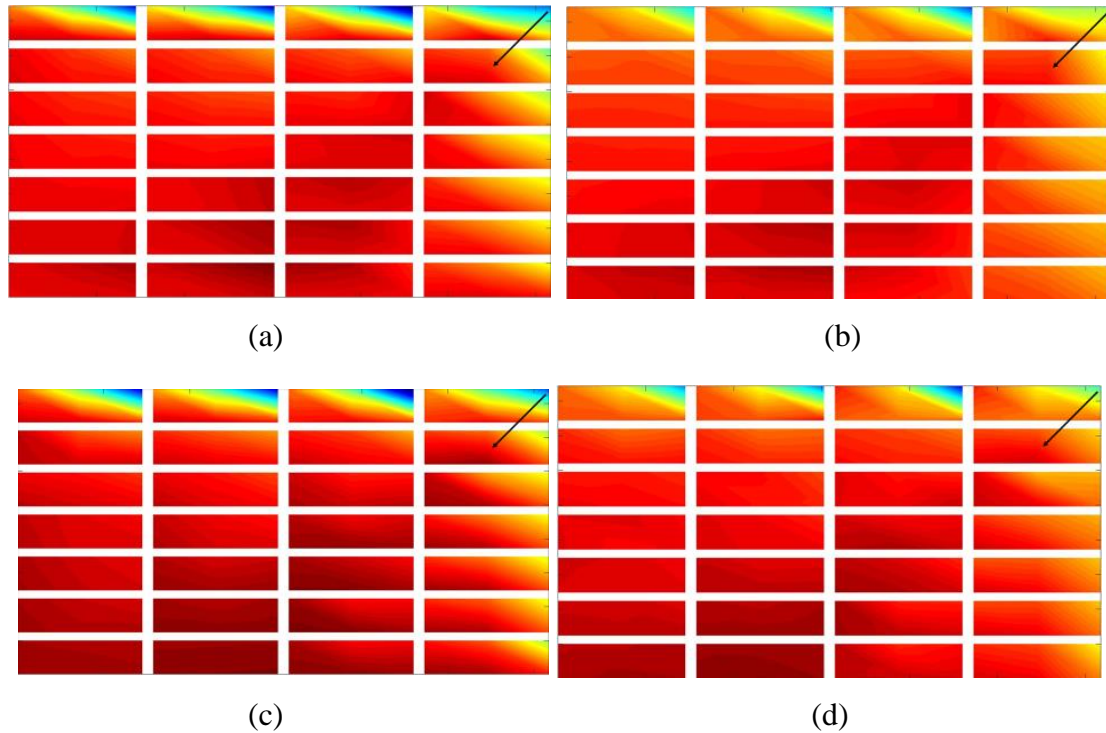


Figure 3-23: Contour map of net pressure distributions for the 225-degree wind direction for (a) experimental and (b) analytical mean net pressures and for (c) experimental and (d) analytical peak net pressures.

The mean as well as peak net pressure distributions from experimental and analytical model, for wind directions of 203, 225 and 315 degrees are shown in Figure 3-22, 3-23 and 3-24. The results showed that for most regions of the panel array, the analytical model is able to predict the mean as well as peak net pressures when compared to the experimental results.

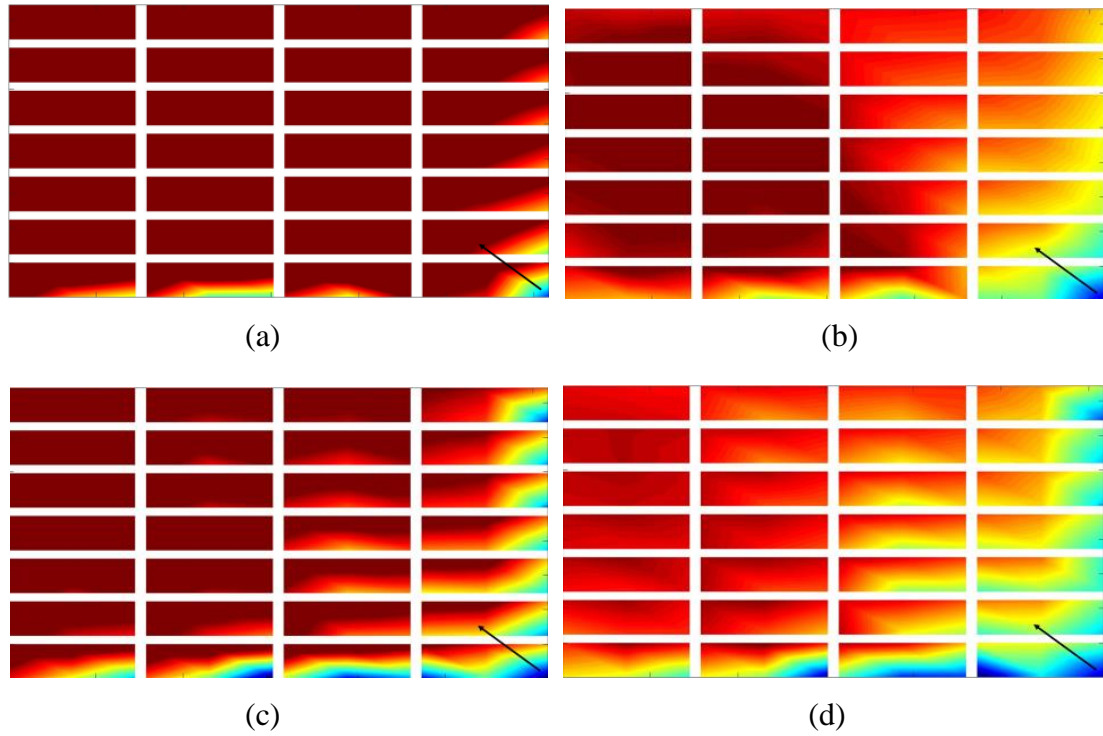


Figure 3-24: Contour map of net pressure distributions for the 315-degree wind direction for (a) experimental and (b) analytical mean net pressures and for (c) experimental and (d) analytical peak net pressures.

3.5.4 Comparison of panel-averaged cavity pressures with predicted time-series

The area-averaged time series of the cavity pressure obtained from the analytical model are also compared with the pressures that are area-averaged over each panel individually. Figure 3-25 shows the comparison of mean as well as peak pressures, for the 135-degree wind direction. The red and blue dots represent the mean and peak results whereas the red and blue lines represent the single values from the analytical model, respectively. The figure shows that the predicted mean area-averaged cavity pressure obtained from the analytical model matches most of the experimental values except at a few locations, where the cavity pressure lack uniformity.

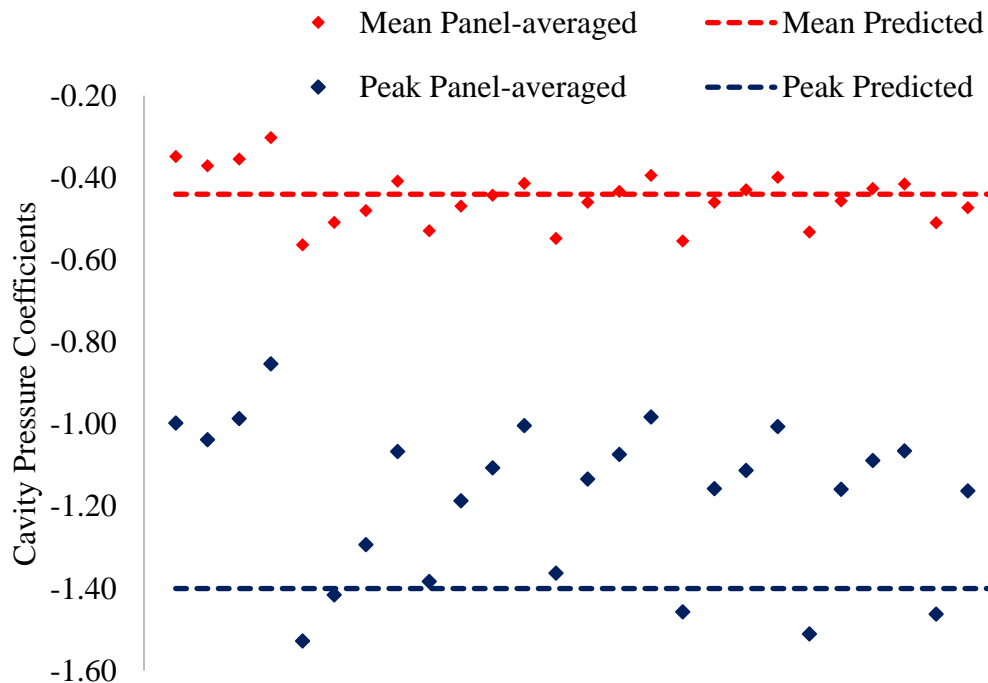


Figure 3-25: Comparison of panel-averaged cavity pressures from the experimental data with the (single) cavity pressure obtained from the analytical model for 135-degree wind direction

In the case of the peak pressures, the predicted values are almost in line with the peak experimental values that are crucial for the design purposes, i.e., the largest magnitude

values. However, there are a few hotspots where the peak panel area-averaged pressures are slightly higher than the predicted values.

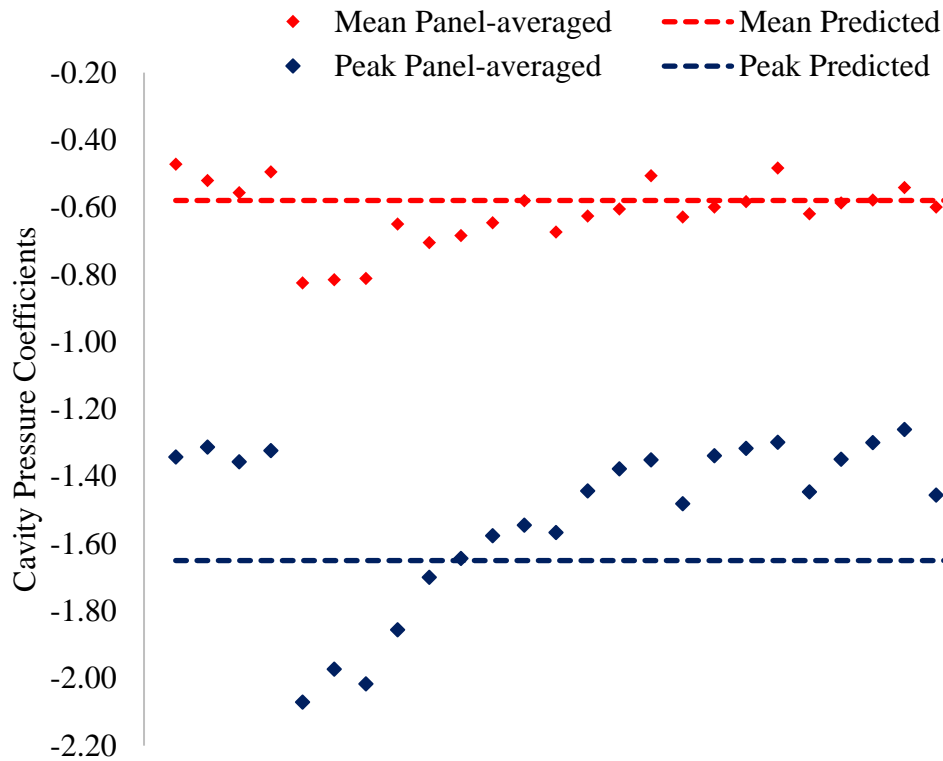


Figure 3-26: Comparison of panel-averaged cavity pressures from the experimental data with the (single) cavity pressure obtained from the analytical model for 203-degree wind direction

Similarly, the comparison of mean and peak panel-averaged cavity pressures for angles 203, 225 and 315-degrees are shown in Figures 3-26, 3-27 and 3-28, respectively. For 203 degrees, there are a few regions where the mean as well as peak loading on certain panels are higher than the predicted results due to some high pressure hot spots in some panels. But the overall pressure distribution looks reasonable. Similarly, a few high pressure zones were observed in certain panels for 225-degree wind direction, but the overall pressure distribution was reasonable.

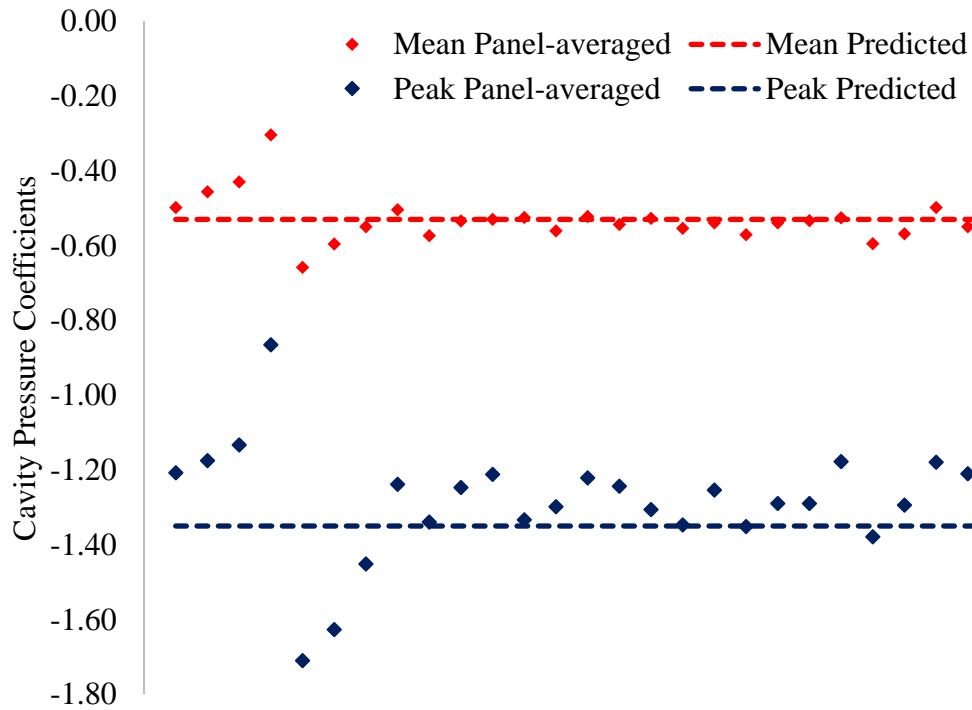


Figure 3-27: Comparison of panel-averaged cavity pressures from the experimental data with the (single) cavity pressure obtained from the analytical model for 225-degree wind direction

For 315-degree wind direction, shown in Figure 3-28, the predicted mean pressure distribution is in good agreement with the actual values, whereas the peak predicted pressures are significantly higher when compared to panel-averaged values. Compared to other wind directions, the gradients in peak net pressures for 315-degree wind direction were high and this has to be investigated.

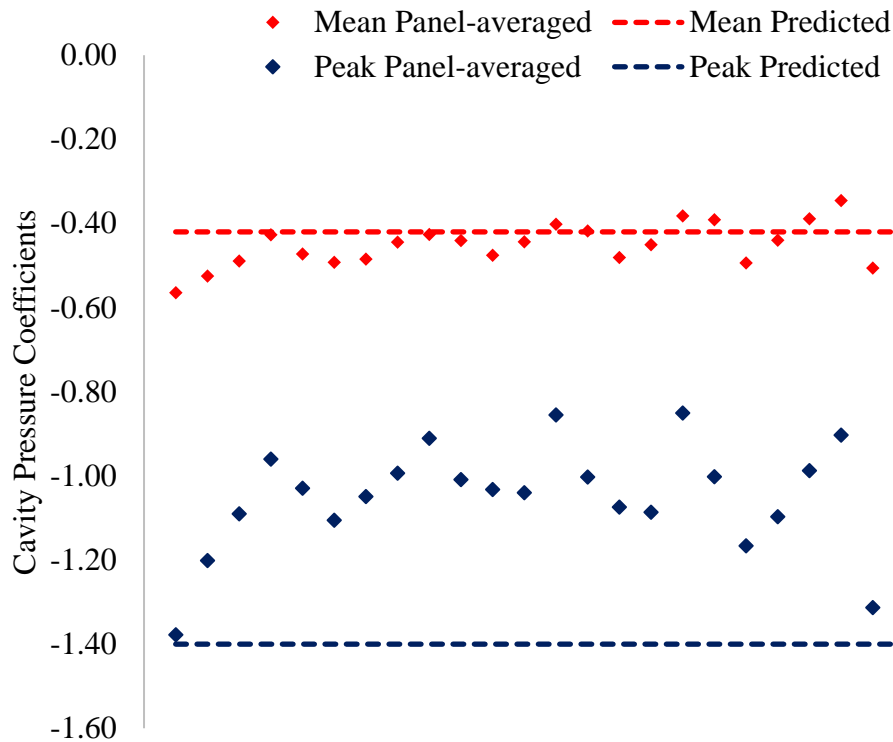


Figure 3-28: Comparison of panel-averaged cavity pressures from the experimental data with the (single) cavity pressure obtained from the analytical model for 315-degree wind direction

3.6 Validation of areas considered in the input for the model

Before proceeding with the results discussion, it is reasonable to make sure that the assumptions considered and the areas taken for the calculation of area-averaged external pressures, which are given as input to the model, are sensible. Hence, a sensitivity analysis was carried out to check the validity of areas considered for the calculation of area-averaged external pressures, for a wind direction of 225 degrees. This check was conducted only for one wind direction, i.e., 225 degrees, since it will be the same for other wind directions also.

Four combinations of areas, as shown in Figure 3-29, are used to estimate the area-averaged external pressures and these external pressures are used as input for the analytical

model to predict the uniform cavity pressures. The details of uniform cavity pressures obtained from the analytical model when the four combinations of external area-averaged pressures were given as input, are given in Table 3-2.

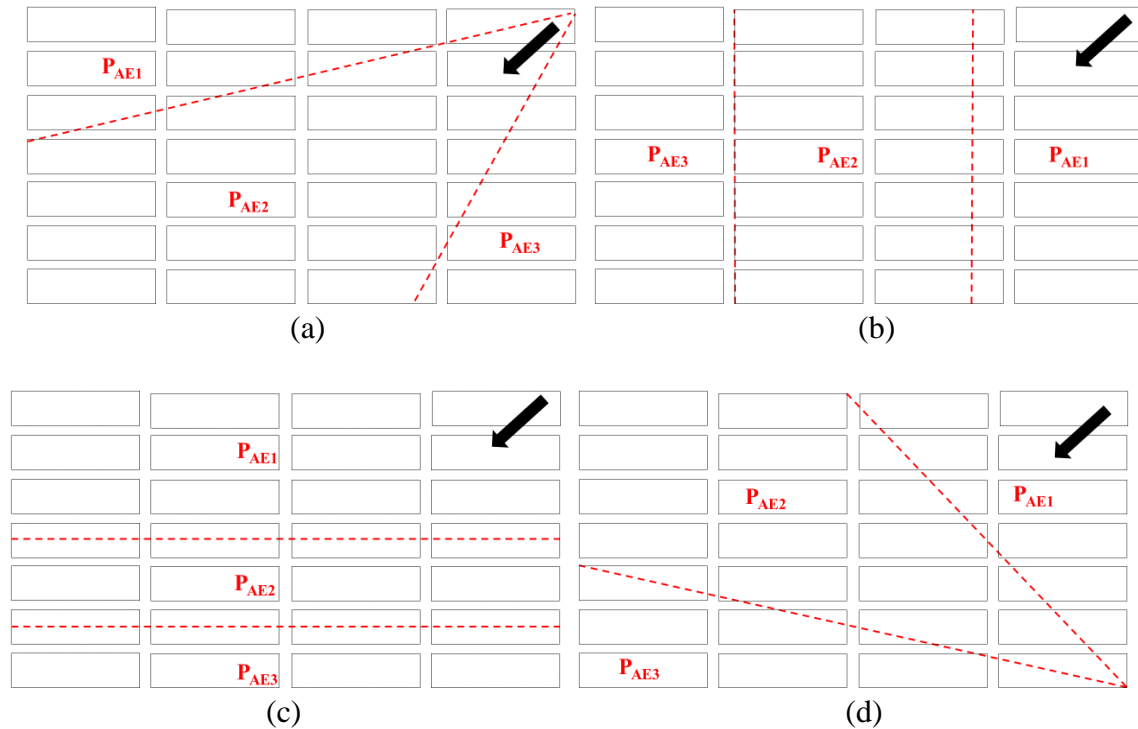


Figure 3-29: Various combinations of external pressures and areas checked for 225 degree wind direction

From Table 3-2, it is obvious that that out of the four combinations, combination “a” is the best combination of areas to be considered for the estimation of area-averaged external pressures. For Combination “a”, most of the ratios of predicted value to the experimental values are within $\pm 10\%$. Moreover, when considering the angle of wind direction, combination “a” is in good agreement with the external pressure distribution pattern. The ratios of predicted values to the experimental results for other combinations like “b”, “c” and “d” are very different, ranging up to almost 40% different.

Table 3-2: Sensitivity of predicted results for various combinations of external pressures for 225-degree wind direction

Combinations	Coefficient of Pressure	Mean	RMS	Max	Min
		Experimental	-0.5380	0.0743	-0.2264
a	Predicted	-0.5180	0.0680	-0.2440	-0.9197
Predicted /Experimental		0.96	0.92	1.08	1.01
b		-0.4250	0.0439	-0.1854	-0.8719
Predicted /Experimental		0.79	0.59	0.82	0.96
c	Predicted	-0.4398	0.0581	-0.1875	-0.8325
Predicted /Experimental		0.82	0.78	0.83	0.91
d		-0.4022	0.0423	-0.1652	-0.8674
Predicted /Experimental		0.75	0.57	0.73	0.95

3.6.1 Sensitivity of the chosen area combination

From Table 3-2, it is clear that out of the 4 combinations, combination “a” is the best option for considering areas for the estimation of area-averaged external pressures. But it is also necessary to make sure how precise the areas need to be to get a reasonably accurate result. For that, a sensitivity study was carried out with combination “a”. Different cases of sensitivity studies were carried out and the areas considered for each of those cases are shown in Figure 3-30. The red lines is the actual combination “a” case explained in the previous section. The green and black lines denote the areas of two case studies considered for checking the sensitivity of the simplified areas chosen. Each of the case studies were carried out by either increasing or decreasing the areas considered for each simplified areas.

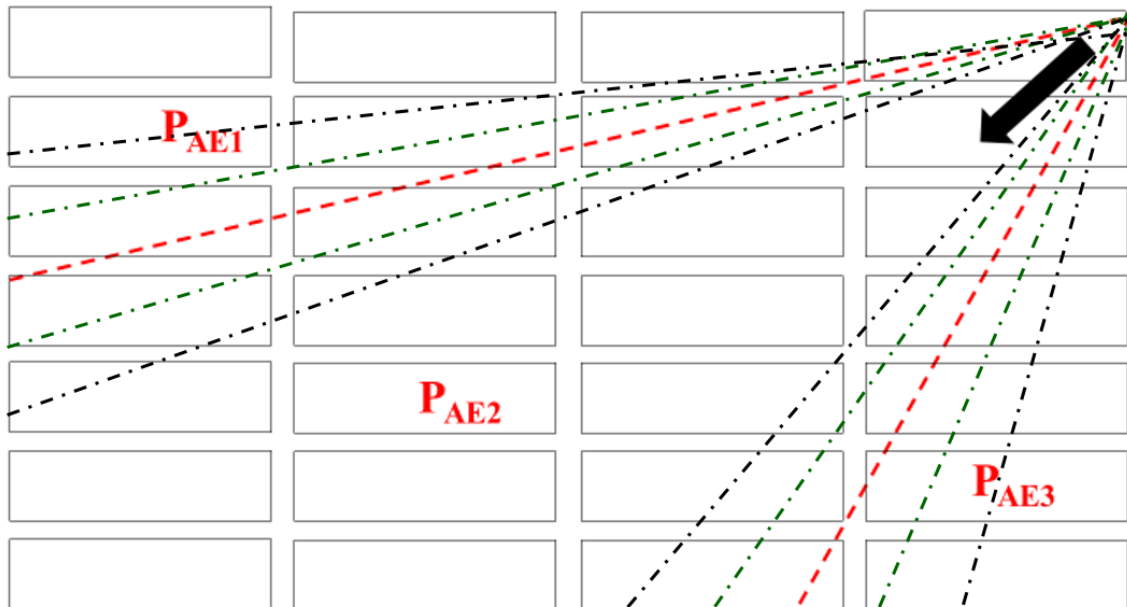


Figure 3-30: Sensitivity cases considered for combination “a” for 225-degree wind direction.

For example, assume that, in the case of combination “a”, the areas considered for the calculation of area-averaged external pressures P_{AE1} , P_{AE2} and P_{AE3} are A, B and C, respectively. In the sensitivity study, these areas are either increased or decreased by 25% and 50% and their various combinations are used, as shown in Table 3-3. The case 1 in Table 3-3 is the combination “a” and case 2 through 13 are the various combinations of areas studied, either by increasing or decreasing the areas.

From the sensitivity study, it is clear that when the areas considered in combination “a” were changed by either increasing or decreasing the simplified areas, the predicted cavity pressure values were varying within a range of around $\pm 14\%$ of the experimental value. So that means, the combination of areas has to be selected based on the external pressure distribution and wind direction. Once a combination is selected based on the above factors, the impact of area changes on the cavity pressure calculation is minimal.

Table 3-3: Sensitivity of predicted results for various combinations of external pressures in combination “a” for 225-degree wind direction

Case	Areas considered for the calculation of area-averaged external pressures			Coefficient of Pressure of predicted cavity pressure			
	P _{AE1}	P _{AE2}	P _{AE3}	Mean	RMS	Max	Min
1	A	B	C	-0.5180	0.0680	-0.2440	-0.9197
2	+25% A	-25% B	C	-0.4869	0.0632	-0.2318	-0.8737
3	+50% A	-50% B	C	-0.4610	0.0612	-0.2147	-0.8001
4	-25% A	+25% B	C	-0.5439	0.0721	-0.2611	-0.9749
5	-50% A	+50% B	C	-0.5698	0.0762	-0.2708	-1.0393
6	+25% A	B	-25% C	-0.4772	0.0620	-0.2295	-0.8650
7	+50% A	B	-50% C	-0.4518	0.0600	-0.2126	-0.7921
8	-25% A	B	+25% C	-0.5330	0.0706	-0.2585	-0.9651
9	-50% A	B	+50% C	-0.5584	0.0746	-0.2681	-1.0289
10	A	+25% B	-25% C	-0.5113	0.0664	-0.2503	-0.9436
11	A	+50% B	-50% C	-0.4841	0.0643	-0.2319	-0.8642
12	A	-25% B	+25% C	-0.5711	0.0757	-0.2741	-1.0209
13	A	-50% B	+50% C	-0.5755	0.0664	-0.2630	-1.0107

Chapter 4

4 Conclusions

4.1 Conclusions

The main objective of this study was to do a proof-of-concept work to assess whether or not the lumped-leakage approach can be used in an analytical model which can predict the cavity pressures in a double-layer system, given user-chosen area-averaged external pressures as input. The method was developed with the assumptions that the cavity volume is well-defined and the cavity pressure is uniform. Both the assumptions were true for the case of the wind tunnel experiment data used for the validation of the model results. An algorithm was developed which explains the working of the analytical model in a step by step manner was also suggested. In this study, the process of selecting the simplified areas, which is the third step in the algorithm was done manually to check whether the concept of lumped leakage could work. The steps for automating the whole process was also suggested in the algorithm. The comparison of results from the analytical model with the experimental results, obtained from Stenabaugh (2015), shows a reasonable agreement. There is good statistical agreement between the predicted results and the experimental ones. The comparison of mean as well as peak loads shows reasonable match between both the results.

4.2 Future Recommendations

As mentioned in the conclusions, the simplified areas selection process in the model was done manually in this study. But to convert this concept to an accurate, practical analytical model, the whole process has to be automated. Moreover, in this study, the wind tunnel experiment data used for the validation of the equations and concept of lumped leakage was taken from a single configuration of solar panel array study. The analytical model has to be compared with a variety of wind tunnel experiment data from different types of double-layer systems.

References

- Aly, A., & Bitsuamlak, G. (2014). Wind-induced pressures on solar panels mounted on residential homes. *Journal of Architectural Engineering*, 20(1): 4013003.
- Amano, T., Fujii, K. and Tazaki, S. (1988). Wind loads on permeable roof-blocks in roof insulation systems. *Journal of Wind Engineering and Industrial Aerodynamics*, 29:39-48.
- Asghari Mooneghi, M., Irwin, P., & Gan Chowdhury, A. (2014). Large-scale testing on wind uplift of roof pavers. *Journal of Wind Engineering and Industrial Aerodynamics*, 128: 22-36.
- Banks, D. (2013). The role of corner vortices in dictating peak wind loads on tilted flat solar panels mounted on large, flat roofs. *Journal of Wind Engineering and Industrial Aerodynamics*, 123: 192-201.
- Banks, D., Merony, R., Sarkar, P., Zhao, Z., & Wu, F. (2000). Flow visualization of conical vortices on flat roofs with simultaneous surface pressure measurement. *Journal of Wind Engineering and Industrial Aerodynamics*, 84: 65-85.
- Baskaran, B., & Brown, W., (1992). Performance of Pressure Equalized Rainscreen Walls under cyclic loading. *Journal of Thermal Envelope and Building Science*, 16: 183-193.
- Baskaran, B., (1994). A Numerical model to evaluate the performance of pressure equalized rainscreen walls. *Building and Environment*, 29: 159-171
- Bienkiewicz, B., & Endo, M. (2009). Wind considerations for loose-laid and photovoltaic roofing systems. 2009 Structures Congress - Don't Mess with Structural Engineers: Expanding Our Role (pp. 2578-2587). Reston, VA: American Society of Civil Engineers.
- Bienkiewicz, B., & Sun, Y. (1992). Wind-tunnel study of wind loading on loose-laid roofing systems. *Journal of Wind Engineering and Industrial Aerodynamics*, 41-44: 1817-1828.
- Bienkiewicz, B., & Sun, Y. (1997). Wind loading and resistance of loose-laid roof paver systems. *Journal of Wind Engineering and Industrial Aerodynamics*, 72(1-3):401-410.
- Bofah, K. K., Gerhardt, H. J., Kramer, C. (1996). Calculations of pressure equilibrium underneath loose-laid, flow permeable roof insulation boards. *Journal of Wind Engineering and Industrial Aerodynamics*, 59: 23-37.

- Boldes, U., Colman, J., Leo, J. M. (2003). About the penetration of a horizontal axis cylindrical vortex into the nearby downwind region of a vertical porous fence. *Journal of Wind Engineering and Industrial aerodynamics*, 91:859-872.
- Briassoulis, D., Mistrionis, A., Giannoulis, A., (2010). Wind forces on porous elevated panels. *Journal of Wind Engineering and Industrial Aerodynamics*, 98: 919-928.
- Browne, M., Gibbons, M., Gamble, S., & Galsworthy, J. (2013). Wind loading on tilted roof-top solar arrays: The parapet effect. *Journal of Wind Engineering and Industrial Aerodynamics*, 123: 202-213.
- Burgess, J. C., (1995). Air pressure equalization in rainscreened joints by geometric alteration. *Building and Environment*, 30: 13-18
- Cao, J., Yoshida, A., Saha, P., & Tamura, Y. (2013). Wind loading characteristics of solar arrays mounted on flat roofs. *Journal of Wind Engineering and Industrial Aerodynamics*, 123: 214-225.
- Chapra, S.C. and Canale, R.P. (2006). *Numerical methods for engineers*. 5th Edition, McGraw-Hill, pp. 632-634.
- Cheung, J.C.K. and Melbourne, W.H. (1988). Wind loading on a porous roof. *Journal of Wind Engineering and Industrial Aerodynamics*, 29: 19-28.
- Choi, E.C.C. and Wang, Z. (1998). Study on pressure-equalization of curtain wall systems. *Journal of Wind Engineering and Industrial Aerodynamics*, 73:251-266.
- Cope, A. D., Crandell, J. H., Johnston, D., Kochkin, V., Liu, Z., Stevig, L., and Reinhold, T. A. (2013). Wind Loads on Components of Multi-Layer Wall Systems with Air-Permeable Exterior Cladding. *Proceedings of ATC & SEI Conference on Advances in Hurricane Engineering*, Miami, Florida, October 24-26, 2012, pp. 238-257.
- Fang, F. M., Wang, D. Y. (1997). On the flow around a vertical porous fence. *Journal of Wind Engineering and Industrial Aerodynamics*, 67&68: 415-424.
- Fazio, P., & Kontopidis, T. (1988). Cavity pressure in rain screen walls. *Building and Environment*, 23: 137-143.
- Fazio, P., & Kontopidis, T., (1988). Cavity Pressure in Rainscreen Walls. *Building and Environment*, 23: 137-143
- Gerhardt, H.J. and Janser, F. (1994). Wind loads on wind permeable facades. *Journal of Wind Engineering and Industrial aerodynamics*, 53:37-48.
- Gerhardt, H.J. and Kramer, C. (1983). Wind loads on wind-permeable building facades. *Journal of Wind Engineering and Industrial Aerodynamics*, 11: 1-20.

- Geurts, C., & Blackmore, P. (2013). Wind loads on stand-off photovoltaic systems on pitched roofs. *Journal of Wind Engineering and Industrial Aerodynamics*, 123:239-249.
- Geurts, C., & Van Bentum, C. (2007). Wind loads on solar energy roofs. *Heron*, 52(3)201-222.
- Geurts, C., & VanBentum, C. (2006). *Wind Loads on Active Roofs: Part 1. Introduction and Classification of Systems 2006-D-R0203*. Delft, Netherlands: Netherlands Organization for Applied Scientific Research (TNO).
- Giannoulis, A., Briassoulis, M. D. (2010). Experimental and numerical investigation of the airflow around a raised permeable panel. *Journal of Wind Engineering and Industrial aerodynamics*, 98:808-817.
- Ginger, J., Payne, M., Stark, G., Sumant, B., & Leitch, C. (2011). *Investigation on Wind Loads Applied to Solar Panels Mounted on Roofs*. Townsville, Australia: Cyclone Testing Station.
- Ginger, J.D., Holmes, J.D. and Kim, P.Y. (2010). Variation of internal pressure with varying sizes of dominant openings and volumes. *Journal of Structural Engineering*, 136(9): 1319-1326.
- Guha, T.K. (2011). *Internal pressure in low and medium rise buildings subjected to high winds*. Doctoral Thesis, The University of Auckland, New Zealand.
- Holmes, J. (2007). *Wind Loading of Structures*. New York, New York: Taylor & Francis.
- Holmes, J.D. (1979). Mean and fluctuating internal pressure induced by wind. *Proceedings of the 5th International Conference on Wind Engineering*, Colorado State University, Fort Collins, Colorado, USA, July, 1979, pp.435-450.
- Inculet, D.R., & Davenport, A.G., (1994). Pressure-equalized rainscreens: A study in the frequency domain. *Journal of Wind Engineering and Industrial Aerodynamics*, 53: 63-87.
- Kala, S., Stathopoulos, T., Kumar, K. S. (2008). Wind loads on rainscreen walls: Boundary-layer wind tunnel experiments. *Journal of Wind Engineering and Industrial Aerodynamics*, 96: 1058-1073.
- Kilip, I R., & Cheetham D W. (1984). The Prevention of rain Penetration through External Walls and joints by means of Pressure Equalization. *Building and Environment*, 19: 81-91
- Kind, R. (1986). Worst suctions near edges of flat rooftops on low-rise buildings. *Journal of Wind Engineering and Industrial Aerodynamics*, 25(1): 31-47.

- Kind, R., & Wardlaw, R. (1982). Failure mechanism of loose-laid roof-insulation systems. *Journal of Wind Engineering and Industrial Aerodynamics*, 9: 325-341.
- Kind, R.J. Savage, M.G. and Wardlaw, R.L. (1988). Prediction of wind-induced failure of loose laid roof cladding systems. *Journal of Wind Engineering and Industrial Aerodynamics*, 29: 29-37.
- Kopp, G. (2013). Wind loads on low profile, tilted, solar arrays placed on large, flat, low rise building roofs. *Journal of Structural Engineering*, 140(2): 04013057.
- Kopp, G., & Banks, D. (2013). Use of the wind tunnel test method for obtaining design wind loads on roof-mounted solar arrays. *Journal of Structural Engineering*, 139(2): 284-287.
- Kopp, G.A., Farquhar, S. and Morrison, M.J. (2012). Aerodynamic mechanisms for wind load on tilted, roof-mounted solar arrays. *Journal of Wind Engineering and Industrial Aerodynamics*, 111: 40-52.
- Kopp, G.A., Oh, J.H. and Incelet, D.R. (2008). Wind-induced internal pressures in houses. *Journal of Structural Engineering*, 134 (7): 1129-1138.
- Kumar, K.S. (2000). Pressure equalization of rainscreen walls: a critical review. *Building and Environment*, 35: 161-179.
- Kumar, K.S., and van Schijndel, A.W.M. (1999), "Prediction of pressure equalization performance of rainscreen walls", *Wind and Structures*, 2(4), 325-345.
- Kumar, K.S., and Wisse, J.A., (2001), "Pressure equalization of rainscreen facades: Analysis of the field data in the frequency domain", *Wind and Structures*, 4, 101-118.
- Kumar, K.S., Stathopoulos, T. and Wisse, J.A. (2003). Field measurement data of wind loads on rainscreen walls. *Journal of Wind Engineering and Industrial Aerodynamics*, 128: 22-36. 91:1401-1417.
- Langmans, J., Desta, T. Z., Alderweireldt, L., Roels, S., (2015). Experimental analysis of cavity ventilation behind residential rainscreen cladding systems. *Energy Procedia*, 78: 1750-1755.
- Lee, S.J. and Kim, H.B. (1998). Velocity field measurement of flow around a triangular prism behind a porous fence. *Journal of Wind Engineering and Industrial aerodynamics*, 77/78:521-530.
- Lee, S.J. and Kim, H.B. (1999). Laboratory measurements of velocity and turbulence field behind porous fences. *Journal of Wind Engineering and Industrial aerodynamics*, 80:311-326.

- Lee, S.J. and Park, C. W. (1999). Surface pressure characteristics on a triangular prism located behind a porous fence. *Journal of Wind Engineering and Industrial aerodynamics*, 80:69-83.
- Lee, S.J. and Park, C. W. (1999). The shelter effect of porous wind fences on coal piles in POSCO open storage yard. *Journal of Wind Engineering and Industrial aerodynamics*, 84:101-118.
- Lee, S.J. and Park, C.W. (1998). Surface-pressure variations on a triangular prism by porous fences in a simulated atmospheric boundary layer. *Journal of Wind Engineering and Industrial aerodynamics*, 73:45-58.
- Letchford, C. W., Row, A., Vitale, A., Wolbers, J. (2000). Mean wind loads on porous canopy roofs. *Journal of Wind Engineering and Industrial aerodynamics*, 84:197-213.
- Lieblein, J. (1974). *Efficient Methods of Extreme-value Methodology*. Washington, D.C.: National Bureau of Standards.
- Lou, W., Huang, M., Zhang, M. and Lin, N. (2012). Experimental and zonal modeling for wind pressures on double-skin facades of a tall building. *Energy and Buildings*, 54:179-191.
- Maffei, J., Telleen, K., Ward, R., Kopp, G., & Schellenberg, A. (2013). Wind design practice and recommendations for solar arrays on low-slope roofs. *Journal of Structural Engineering*, 140(2): 04013040.
- Mas, A., Gutierrez, J., Gil, E., Gil, A., Galvan, V., (2011). Design and construction recommendations to improve impermeability in rainscreen walls built with natural stone coverings. *Journal of Wind Engineering and Industrial Aerodynamics*, 25: 1753-1761.
- Nederlands Normalisatie – Instituut. (2013). *NEN 7250 Solar Energy Systems Integration in Roofs and Facades – Building Aspects*. Ontwerp, Netherlands: Nederlands Normalisatie – Instituut.
- Oh, J., & Kopp, G. (2014). Modelling of spatially and temporally-varying cavity pressures in air permeable, double-layer roof systems. *Building and Environment*, 82: 135-150.
- Oh, J., & Kopp, G. (2015). An experimental study of pressure distributions within an air permeable, double-layer roof system in regions of separated flow. *Journal of Wind Engineering and Industrial Aerodynamics*, 138: 1-12.
- Oh, J., Kopp, G.A., and Inculet, D. R. (2007). The UWO contribution to the NIST aerodynamic database for wind loads on low buildings: Part 3. Internal Pressures. *Journal of Wind Engineering and Industrial Aerodynamics*, 95: 755-779.

- Oh, J.H. (2014). Wind-Induced pressures in air permeable, double-layer roof systems in regions of separated flow. Doctoral Thesis, The University of Western Ontario, Canada.
- Okada, H., & Okabe, M. (1991). Wind tunnel tests to determine the wind forces on roof blocks for existing buildings. *Journal of Wind Engineering and Industrial Aerodynamics*, 38: 393-403.
- Pratt, R., & Kopp, G. (2013). Velocity measurements around low-profile, tilted, solar arrays mounted on large flat-roofs, for wall normal wind directions. *Journal of Wind Engineering and Industrial Aerodynamics*, 123(2): 226-238.
- Richardson, G.M. and Richards, P.J. (1995). Full-Scale measurement of the effect of a porous windbreak on wind spectra. *Journal of Wind Engineering and Industrial aerodynamics*, 54/55:611-619.
- Richardson, G.M. and Richards, P.J. (1999). Wind loads on porous structures. *Journal of Wind Engineering and Industrial aerodynamics*, 83:455-465.
- Robertson, A. P., Roux, P., Gratraud, J., Scarascia, G., Castellano, S., Virel, M. D., Palier, P. (2002). Wind pressures on permeably and impermeably-clad structures. *Journal of Wind Engineering and Industrial aerodynamics*, 90:461-474.
- SEAO Solar Photovoltaic Systems Committee. (2012). SEAO PV2-2012 Wind Design for Low-profile Solar Photovoltaic Arrays on Flat Roofs. Sacramento, California: Structural Engineers Association of California.
- Sharma, R.N. and Richards, P.J. (1997). Computational modelling of transient response of building internal pressures to a sudden opening. *Journal of Wind Engineering and Industrial Aerodynamics*, 72: 149-161.
- Shiau, B. S., (1998). Measurement of turbulence characteristics for flow past porous windscreen. *Journal of Wind Engineering and Industrial Aerodynamics*, 74-76: 521-530.
- Stathopoulos, T., Zisis, I., Xypnitou, E., (2014). Local and overall wind pressure and force coefficients for solar panels. *Journal of Wind Engineering and Industrial Aerodynamics*, 125: 195-206.
- Stenabaugh, S., (2015). Design Wind Loads for Solar Modules Mounted Parallel to the Roof of a Low-rise Building. Doctoral Thesis, The University of Western Ontario, Canada, 2015.
- Stenabaugh, S., Iida, Y., Kopp, G. & Karava, P. (2015). Wind loads on photovoltaic arrays mounted parallel to sloped roofs on low-rise buildings. *Journal of Wind Engineering and Industrial Aerodynamics*, 139: 16-26.

- Stenabaugh, S., Karava, P., & Kopp, G. (2010). Design Wind Loads for Photovoltaic Systems on Sloped Roofs of Residential Buildings. London, Canada: Boundary Layer Wind Tunnel Laboratory.
- Stenabaugh, S., Karava, P., & Kopp, G. (2011). Design wind loads for photovoltaic systems on sloped roofs of residential buildings. 13 ICWE. Amsterdam, Netherlands.
- Sun, Y. and Bienkiewicz, B. (1993). Numerical simulation of pressure distributions underneath roofing paver systems. *Journal of Wind Engineering and Industrial Aerodynamics*, 46-47: 517-626.
- Tieleman, H., Akins, R., & Sparks, P. (1980). An investigation of wind loads on solar collectors. Blacksburg, VA: Virginia Polytechnic Institute and State University.
- Trung, V.T., Tamura, Y. and Yoshida, A. (2010). Numerical computation for lower surface pressures on a porous sunshade roof cover sheet. *Proceedings of the 5th International Symposium on Computational Wind Engineering*, Chapel Hill, North Carolina, USA, May 23-27, 2010.
- Van Schijndel, A.W.M. and Schols, S.F.C. (1998). Modeling pressure equalization in cavities. *Journal of Wind Engineering and Industrial Aerodynamics*, 74-76:641-649.
- Vickery, B.J. (1986). Gust factors for internal pressures in low-rise buildings. *Journal of Wind Engineering and Industrial Aerodynamics*, 23: 259-271.
- White, F.M., *Fluid Mechanics*, 4th edition. 1999, New York, USA: McGraw-Hill.
- Xie, J., Schuyler, G.D. and Resar, H.R. (1992). Prediction of net pressure on pressure equalized cavities. *Journal of Wind Engineering and Industrial Aerodynamics*, 41-44: 2449-2460.

Appendix A: Summary of previous research on pressure equalization

Author	Year	Building Geometry	Scale	Contribution
Gerhardt and Kramer	1983	Width = 2 m, Height = 1.6 m	None	Wind loads on wind permeable facades of low-rise buildings
Cheung and Melbourne	1986	1.21 * 1.21 * 0.2 m	None	The effects of porosity and internal volume on the mean, standard deviation and peak pressures on a porous surface
Amano and Fujii	1988	3.45 * 3.45 * 1.48 m	None	The internal pressure distribution under a known external pressure field
Gerhardt and Janser	1994	None	1:350	Wind loading on a porous façade systems
Richardson and Richards	1995	1.83 * 1.05 m Depth = 2m	None	Streamwise turbulence spectra in the vicinity of a porous windbreak
Bofah et al.	1996	None	None	The flow underneath a loosely laid insulation board or a paver
Fang and Wang	1997	None	None	The turbulent flow around a vertical porous fence was
Lee and Kim	1998	Height = 25 mm B/H = 0.012	None	The shelter effect of a porous wind fence on a triangular prism

Author	Year	Building Geometry	Scale	Contribution
Lee and Park	1998	Height = 25 mm B/H = 0.012	None	Surface-pressure variations on a two-dimensional triangular prism model behind porous wind fences.
Shiau	1998	3 mm thickness 10 cm high 300 cm long	None	Measurements of the turbulence characteristics for a turbulent boundary layer flow past porous windscreen
Lee and Kim	1999	Height = 40 mm Width = 300 mm Thickness = 4 mm	None	Flow characteristics of turbulent wake behind porous fences
Lee and Park	1999	Height = 40 mm Breadth = 95 mm Depth = 0-120 mm	None	The shelter effect of porous wind fences on wind-blown dust
Richards and Robinson	1999		None	The factors that determine the wind load on porous structures
Lee and Park	2000	Height = 40 mm Breadth 95 mm Depth = 0-120 mm	None	The shelter effect of porous wind fences on surface pressure and wall shear stress
Letchford et al.	2000	Breadth 300 mm Depth 300 mm	1:50	Mean overall lift and drag forces on a range of canopy or open roof forms with varying porosities
Robertson et al.	2002	Height = 1.83 m Breadth = 4 m Depth = 4 m	1:2	The pressure coefficient data for cladding.
Boldes et al.	2003	Height = 20 cm	1:15	A cylindrical vortex embedded in a low turbulence stationary horizontal stream, running through a two-dimensional narrow vertical woven fence located on the

Author	Year	Building Geometry	Scale	Contribution
Trung et al.	2009	200 mm high (H) 470 mm wide (B) 710 mm deep	1:50	The effects of parapet and underneath volume on wind loading on porous roof cover sheets
Briassoulis et al.	2010	Height = 5m Width = 7m Depth = 2m	None	The wind pressures on experimental scale panels covered by various types of nets
Giannoulis and Briassoulis	2010	Height = 3 m Width = 7m Depth = 2m	None	The analysis of air flow around an elevated permeable panel
Trung et al.	2010	200 mm high 470 mm wide 710 mm deep	1:50	The lower surface pressures on a porous sunshade roof cover sheet with respect to two porosities
Cope et al.	2013	30 * 40*17 ft	None	Wind pressure loading on layers of exterior wall assemblies that include vinyl siding, insulation in the wall cavity and gypsum board interior sheathing
Cope et al.	2013	30 * 40*17 ft	None	The loads on the fasteners used to attach the siding to the wall
Oh and Kopp	2014		1:30	Time-varying pressure distributions in the cavity of air-permeable layer, double-layer systems
Oh and Kopp	2015		1:30	The effects of the gaps between panels (G), cavity depth between layers (H), and the panel size (L) on the pressures and panel loads
Killip and Cheetham	1984	None	None	A theory on pressure equalizing rain-screen wall

Author	Year	Building Geometry	Scale	Contribution
Pazio and Kontopidis	1988	2.4*3.6*2.6 m	None	The correlation among cavity pressure, wind pressure and openings
Baskaran and Brown	1992	1.5*1.5*2.1 m	None	An analytical model to simulate PER wall performance
Baskaran	1994		None	A numerical model to simulate the performance of the Pressure equalized rainscreen walls
Inculet and Davenport	1994	0.6*0.6*0.6 m	1:12	The effect of venting area, air barrier leakage, cavity volume and compartment size
Burgess	1995	635*750*960 mm	None	The effect of joint opening area and joint cavity volume
Burgess	1995	None	None	A numerical model to solve the governing equations of pressure equalization.
Kumar and Schijndel	1999	1*1.3 m	None	Two theoretical models (based on mass balance and Helmholtz resonant theory)
Kumar	2000	None	None	Investigated all the previous research works on pressure equalization of rain screen walls
Kumar and Wisse	2001	167*20*44.6 m	None	Frequency domain analysis to understand the pressure equalization of rain screen walls

Author	Year	Building Geometry	Scale	Contribution
Kumar et al.	2003	1*1.3 m	None	Full scale measurements of wind loading on rainscreen walls
Kala et al.	2008	167*20*44.6 m	None	Parameters affecting the pressure equalization were discussed.
Mas et al.	2011	0.6*0.9 m	None	The performance of rain screen walls when water gets into contact with the façade.
Langmans et al.	2015	2.7*1 m	None	The impact of various cladding materials and the size of ventilation openings on residential rainscreen cladding systems

Appendix B: Numerical Method

As mentioned in section 2.3 of chapter 2, the ordinary differential equations used in the analytical model can be solved by a 2nd order backward differencing numerical method (Chapra and Canale, 2006).

In this method, the derivative term can be assumed as

$$U_t = \frac{3U(t) - 4U(t-1) + U(t-2)}{2h} \quad (A.1)$$

where $t = 1, 2, \dots, n$ is the time index and h is the time step between t and $t-1$.

By substituting the term A.1 in the original equations make them a set of non-linear simultaneous equations and to solve them the non-linear term in the equation i.e., $U_g(t)|U_g(t)|$ is linearized by assigning an approximate value for $|U_g(t)|$. By doing so, the non-linear equations become four simultaneous linear equations with four unknowns i.e., $U_{g1}(t)$, $U_{g2}(t)$, $U_{g3}(t)$ and $P_i(t)$. Now these simultaneous linear equations can be solved for the given area-averaged external pressure data, $P_{AE1}(t)$, $P_{AE2}(t)$, $P_{AE3}(t)$ and also for the initial values of the $U_g(t-1)$ and $U_g(t-2)$. After solving the equations, the obtained $U_g(t)$ should be similar to assumed approximate value for $|U_g(t)|$. If not, a new approximate value for $|U_g(t)|$ should be assumed and the equations are solved. The new assumed approximate value can be taken as $0.5U_g(t) + 0.5|U_g(t)|_{old}$. This computation process will be continued until the solution of $U_g(t)$ and $|U_g(t)|$ are converged.

Curriculum Vitae

Name: Rahul Prabhakaran Nair Sreedevi

Post-secondary Education and Degrees: Anna University
Chennai, Tamil Nadu, India
2002-2006 B.E. (Mechanical Engineering)

University of Kerala
Trivandrum, Kerala, India
2006-2008 M.Tech (Machine Design)

Related Work Experience Project Engineer
RWDI Consulting Engineers and Scientists India (Pvt.) Ltd
2008-2015

Teaching Assistant
The University of Western Ontario
2015-2017

Conference Publications:

Aswin Kumar, Rahul P S, K. Suresh Kumar (2013), Performance optimization of tall buildings subjected to wind – An Indian scenario, 8th Asia-Pacific Conference on Wind Engineering, Chennai, India.

K. Suresh Kumar, Rahul P S, Valerie Sifton (2012), Assessment of Wind Directionality in metropolitan cities in India, 6th National Conference on Wind Engineering, Central Road Research Institute, New Delhi, India.

Krishna Chaithanya, Rahul P S, Suresh Kumar (2014), Wind-Induced response of tall buildings: Comparison of Indian code with American, Canadian and Australian codes, Structural Engineering Convention 2014, IIT Delhi, India.

Rahul P S, Jayaraj Kochupillai (2008), Finite element based analysis of Magnetorheological Damper, National Conference on Technological Trends, College of Engineering Trivandrum, India.